

**OPTIMIZATION OF SPIRAL BASED STRUCTURES FOR  
STRETCHABLE ELECTRONICS**

BY

**Mutee Ur Rehman**

A Thesis Presented to the  
DEANSHIP OF GRADUATE STUDIES

**KING FAHD UNIVERSITY OF PETROLEUM & MINERALS**

DHAHRAN, SAUDI ARABIA

In Partial Fulfillment of the  
Requirements for the Degree of

**MASTER OF SCIENCE**

In

**ELECTRICAL ENGINEERING**

May 2017

KING FAHD UNIVERSITY OF PETROLEUM & MINERALS  
DHAHRAN- 31261, SAUDI ARABIA  
DEANSHIP OF GRADUATE STUDIES

This thesis, written by **Mutee Ur Rehman** under the direction his thesis advisor and approved by his thesis committee, has been presented and accepted by the Dean of Graduate Studies, in partial fulfillment of the requirements for the degree of **MASTER OF SCIENCE IN ELECTRICAL ENGINEERING**.




Dr. Ali Ahmad Al-Shaikhi  
Department Chairman




Dr. Salam A. Zummo  
Dean of Graduate Studies

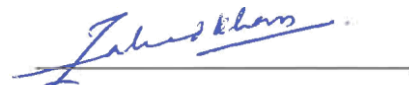
29/8/18  
Date



Dr. Jhonathan Prieto Rojas  
(Advisor)



Dr. Khurram Karim Qureshi  
(Member)



Dr. Mohammed Zahed Mustafa  
Khan  
(Member)

© Mutee Ur Rehman

2017

## ACKNOWLEDGMENTS

First of all, I would like to express my gratitude to my thesis advisor Dr. Jhonathan Prieto Rojas for his continuous support and motivation. He has always been very encouraging and welcoming. He has been very kind and great research mentor who taught me how to conduct the research and to be more creative. This work would never have been possible without his encouragement and constant support. I am also very thankful to him for providing me the opportunity to work at the fabrication facility in KAUST. I would also like to thank him for his help and support during my stay at KAUST especially for first three weeks. He will be a source of inspiration and motivation throughout my career.

I would also like to thank Galo Torres Sevilla for his time, help and guidance for the fabrication process. He has been very kind, supportive and helping throughout my stay at KAUST. He trained me on several tools that were required for the fabrication process for which I am very grateful. Without his help, I might not have been able to complete the work in time.

I am also very thankful to Prof. Muhammad Mustafa Hussain for allowing me to work in his lab at KAUST and to experience the research environment there. I am sure what I learnt there will help me throughout my career. I am also very grateful to Melvin Cruz in Integrated Nanotechnology Lab for his support and help. Moreover, I am thankful to staff in the cleanroom facility at KAUST.

Finally, I am very thankful to my family for their encouragement and motivation.

# TABLE OF CONTENTS

ACKNOWLEDGMENTS.....	IV
TABLE OF CONTENTS .....	V
LIST OF FIGURES.....	VII
LIST OF TABLES.....	X
LIST OF ABBREVIATIONS.....	XI
ABSTRACT .....	XII
ملخص الرسالة.....	XIV
<b>1 CHAPTER INTRODUCTION.....</b>	<b>1</b>
<b>2 CHAPTER LITERATURE REVIEW .....</b>	<b>4</b>
<b>2.1 Mechanics of Flexible Electronics .....</b>	<b>4</b>
<b>2.1.1 Engineering Stress and Strain .....</b>	<b>5</b>
<b>2.1.2 Basic Properties of a Material .....</b>	<b>7</b>
<b>2.1.3 Toughness .....</b>	<b>8</b>
<b>2.1.4 Tensile Test .....</b>	<b>9</b>
<b>2.1.5 True Stress-Strain.....</b>	<b>11</b>
<b>2.1.6 Interaction Between Rigid and Brittle Materials .....</b>	<b>12</b>
<b>2.1.7 Paths to Flexible Electronics.....</b>	<b>14</b>
<b>2.1.8 Structures.....</b>	<b>18</b>

2.1.9	Thin Films .....	25
3	CHAPTER RESULTS AND DISCUSSION .....	32
3.1	Simulation Workflow .....	33
3.2	Simulation Environment.....	35
3.2.1	Standard Spiral Structure .....	36
3.2.2	Spiral with Unequal Halved Serpentine Arms .....	41
3.2.3	Spiral with Equal Halved Serpentine Arms .....	48
4	CHAPTER FABRICATION .....	55
4.1	Fabrication Process Description .....	55
4.1.1	Mask Design.....	55
4.1.2	Fabrication Process For Si (100) Wafer .....	57
4.1.3	Fabrication Process For SOI Wafer .....	65
5	CHAPTER CONCLUSION AND FUTURE WORK .....	68
	REFERENCES .....	70
	VITAE .....	77

## LIST OF FIGURES

Figure 1 Schematic of measurements of the stress [16] .....	7
Figure 2 Comparison of fracture toughness between different materials [17] .....	8
Figure 3 Engineering stress –strain curve for ductile materials [17] .....	10
Figure 4 Illustration of necking in Ductile materials [17] .....	12
Figure 5 Illustration of a device under tensile and compressive stress and presence of mechanically neutral plane [17] .....	12
Figure 6 Allotropes of carbon, two-dimensional graphene (right), quasi-zero-dimensional buck-minsterfullerene (left), and quasi-one-dimensional armchair nanotube (middle) [39].....	17
Figure 7 (a) Silicon membrane in wavy structure ((~100-nm thickness), (b) wavy shape silicon bonded on an elastomer .....	20
Figure 8 (a) Array of silicon NRs in wavy configuration (b) schematic of 1D Bucked NRs bonded on elastomer at troughs [47] .....	20
Figure 9 (a) General illustration of the flexible electronics in mesh structure in stretched form and (b) un-stretched form [55].....	20
Figure 10 (a) Non-coplanar mesh design on elastomer (b) mesh serpentine structure under strain [15] .....	21
Figure 11 Schematic of 2D network of silicon Islands with spring spiral interconnects [62] .....	22
Figure 12 (a) hexagonal islands with spring spiral interconnect (b) the spiral interconnect between the islands [28] .....	22
Figure 13 S-shaped micro-fabricated suspensions when no pressure was applied to the membrane [66] .....	25
Figure 14 Fabrication process flow for releasing silicon pieces from mono-crystalline silicon wafer [75].....	28
Figure 15 Fabrication process flow for releasing double arm spiral structure from SOI wafer [28]. .....	29
Figure 16 Spiral Structures with straight arms (a) spiral structure with two arms, (b) stress distribution along the arms (c) stress distribution along the arms (d) Von misses stress along the arms (e) percentage strain distribution along the arms .....	37
Figure 17 Spiral Structures with triangular-like ends (a) spiral structure with two arms, (b) stress distribution along the arms (c) strain distribution along the arms (d) Von misses stress along the arms (e) percentage strain distribution along the arms. ....	38
Figure 18 Comparison of Spiral structures (a) spiral structure with triangular ends with extended arms(b) comparison of stress distribution among two versions of spiral structure (c) comparison of stress distribution among two versions of spiral structure .....	40
Figure 19 Spiral structures with serpentine arms with trough’s radius bigger than crest (a) spiral structure with serpentine arms having unequal halves(b) stress distribution	

	along the arms, (c) strain distribution along the arms (d) Von-Mises stress along the arms, (e) percentage distribution along the arms.....	42
Figure 20	Spiral Structures with serpentine arms and triangular-like ends (a) spiral structure with two serpentine arms having unequal halves and with triangular-like ends, (b) stress distribution along the arms (c) strain distribution along the arms (d) Von-Mises stress along the arms, (e) percentage strain distribution along the arms .....	43
Figure 21	Spiral-serpentine compound structure with arm's thickness gradually decreasing at the start (a) spiral-serpentine compound structure with modified arm's start, (b) stress distribution along the arms (c) strain distribution along the arms, (d) Von-Mises stress along the arms, (e) percentage strain distribution along the arms. ....	45
Figure 22	Spiral-serpentine compound structure with arm's thickness gradually increasing at the ends (a) spiral-serpentine compound structure with modified arm's end, (b) stress distribution along the arms (c) strain distribution along the arms (d) Von-Mises stress along the arms (e) percentage strain distribution along the arms. ....	46
Figure 23	Spiral structures with serpentine arms with trough's radius smaller than crest (a) spiral structure with serpentine arms having unequal halves (b) stress distribution along the arms (c) strain distribution along the arms (d) Von-Mises stress along the arms (e) percentage strain distribution along the arms.....	47
Figure 24	Spiral structures with serpentine arms having trough's radius equal to crest's radius (a) spiral structure with serpentine arms having equal halves (b) stress distribution along the arms (c) strain distribution along the arms (d) Von-Mises stress along the arms, (e) percentage strain along the arms. ....	49
Figure 25	Comparison of Spiral-serpentine compound structure with equal and unequal halves (a) spiral-serpentine compound structure with serpentine arms having unequal halves(b) spiral-serpentine compound structure with serpentine arms having equal halves (c) comparison of Von Mises stress along the arms (d) comparison of percentage strain distribution along the arms.....	50
Figure 26	Spiral-serpentine compound structure with equal serpentine halves and horseshoes at the end/beginning of arms. Schematics of (a) serpentine/spiral structure with horseshoe at the end, and (b) with horseshoe at the start. (c) Stress comparison along the arms, (d) strain distribution comparison along the arms.....	52
Figure 27	Spiral-serpentine compound structure with equal serpentine halves and horseshoes at the beginning and end of the arms. Schematics of (a) serpentine/spiral structure with two arms and horseshoe structure, and (b) stretched structure. (c) 3D stress distribution along the arms, and (d) 3D strain distribution along the arms. (e) Stress comparison between original spiral and compound structure along their arms, and (f) strain distribution comparison between original spiral and compound structure along their arms.....	53
Figure 28	Summary of the spiral based designs .....	54
Figure 29	Hexagon interconnected thorough single turn spirals .....	56
Figure 30	Hexagon interconnected thorough multi-turn spirals.....	56
Figure 31	Hexagon interconnected thorough single turn.....	57



Figure 32 Fabrication flow for releasing Spiral-serpentine structure from mono-crystalline silicon wafer. ....	58
Figure 33 SEM of the DRIE for mono-crystalline Silicon. ....	60
Figure 34 SEM of spiral interconnects after DRIE for mono-crystalline Silicon.....	60
Figure 35 SEM of the spiral structure after DRIE for mono-crystalline silicon.....	61
Figure 36 SEM of spiral with Island after DRIE for mono-crystalline Silicon.....	61
Figure 37 SEM of spiral after release. ....	62
Figure 38 SEM of the Square Island after release .....	63
Figure 39 SEM of the spiral's horseshoe after release. ....	63
Figure 40 Structure released from mono-crystalline Silicon. ....	64
Figure 41 Structure released from mono-crystalline Silicon. ....	64
Figure 42 Fabrication process flow for the silicon on insulator (SOI) wafer. ....	65
Figure 43 SOI wafer after the DRIE of Silicon. ....	66
Figure 44 Released Square structure from SOI wafer. ....	67
Figure 45 Stretched spiral between two Square Islands. ....	67

## LIST OF TABLES

Table 1 Main properties of common polymers.....	30
Table 2 Main properties of common conductors and semiconductors .....	31

## LIST OF ABBREVIATIONS

<b>CNTs</b>	.....	Carbon Nanotubes
<b>CB</b>	.....	Carbon Black
<b>CMOS</b>	.....	Complementary Metal Oxide Semiconductor
<b>DRIE</b>	.....	Deep Reactive Ion Etching
<b>EGaIn</b>	.....	Eutectic Gallium Indium
<b>FEA</b>	.....	Finite Element Analysis
<b>IoE</b>	.....	Internet-of-Everything
<b>IOT</b>	.....	Internet-of-Things
<b>ITO</b>	.....	Indium Tin Oxide
<b>NRs</b>	.....	Nanoibbons
<b>PDMS</b>	.....	Polydimethylsiloxane
<b>PET</b>	.....	Polyethylene terephthalate
<b>PI</b>	.....	Polyimide
<b>RIE</b>	.....	Reactive Ion Etching
<b>SiO<sub>2</sub></b>	.....	Silicon Dioxide
<b>SOI</b>	.....	Silicon-on-Insulator
<b>SWCNTs</b>	.....	Single wall carbon nanotubes
<b>TCO</b>	.....	Transparent Conducting Oxides
<b>TEG</b>	.....	Thermoelectric Generator
<b>UTS</b>	.....	Ultimate Tensile Strength
<b>UTB-SOI</b>	.....	Ultra-thin body silicon on insulator
<b>XeF<sub>2</sub></b>	.....	Xenon Difluoride

## **ABSTRACT**

Full Name : Mutee Ur Rehman  
Thesis Title : Optimization of Spiral Based Structures for Stretchable Electronics  
Major Field : Master of Science in Electrical Engineering  
Date of Degree : May, 2017

Stretchable electronics is a rising technology, promising to replace the conventional brittle and rigid electronics for applications that demand mechanical compliance to irregular, complex and mobile shapes. Several approaches have been proposed to find an optimum balance between electrical and mechanical characteristics. These include finding new flexible electronic materials, integrating both organic and inorganic materials or incorporating structural modifications to conventional materials, thus achieving flexibility and stretchability. Silicon based electronic devices are still dominant in the market due to the very mature technology of conventional electronics. Therefore, it will be more practical to have stretchable/ flexible devices using the conventional electronic materials. Structural modifications to these materials can lead to achieve the desired electronic devices, compliant according to the application. Previously, the use of spiral-based structures made entirely out of silicon, a well-mature and high-performing material, has been proposed as a platform for ultra-stretchable electronic applications. In this research work we have demonstrated the use of spiral-based compound, fractal-inspired structures to optimize and greatly reduce the stress and strain distribution along them. The integration of double-arm spirals with variants of serpentine and horseshoe structures has been considered and their mechanical response to an applied deformation has been performed through finite element analysis. The proposed compound structures provide outstanding stretching capabilities and demonstrate up to 58% reduction in stress/strain, as well as a more uniform distribution as compared to the initial, un-optimized spiral-

based structure. These results show the remarkable potential of combining structures to optimize their mechanical behavior, thus accomplishing more robust platforms that will leverage the development of stretchable electronics. Moreover, the designed structures were also fabricated using conventional microfabrication techniques for bulk Si (100) and Silicon on Insulation (SOI) wafers, respectively. Finally, the fabricated spiral-based structure was subjected to approximately 470% strain, to confirm the effectiveness of the fabricated process.

## ملخص الرسالة

الاسم الكامل: مطيع الرحمن

عنوان الرسالة: استمثال البنى اللولبية للاستخدام في الإلكترونيات القابلة للشد

التخصص: الهندسة الكهربائية

تاريخ الدرجة العلمية: مايو 2017م

إن الإلكترونيات القابلة للتمدد هي تقنية متطورة، وواحدة لتحل محل الإلكترونيات التقليدية الهشة والقاسية للتطبيقات التي تتطلب التوافق والمطاوعة الميكانيكية مع الأشكال غير المنتظمة والمعقدة والمتنقلة. وقد اقترحت عدة طرق لإيجاد التوازن الأمثل بين الخصائص الكهربائية والميكانيكية. وتشمل هذه الطرق إيجاد مواد إلكترونية مرنة جديدة، ودمج المواد العضوية وغير العضوية معاً، أو إدخال تعديلات هيكلية على المواد التقليدية، وبالتالي تحقيق المرونة والتمدد. لا تزال الأجهزة الإلكترونية القائمة على السيليكون مهيمنة في السوق بسبب التكنولوجيا المتقدمة جداً للإلكترونيات التقليدية. ولذلك سيكون تصنيع الأجهزة المرنة و المتعددة باستخدام المواد الإلكترونية التقليدية ذا جدوى عملية أكثر. التعديلات الهيكلية لهذه المواد يمكن أن تؤدي إلى الحصول على الأجهزة الإلكترونية المرنة والمطاوعة المطلوبة حسب للتطبيق. في السابق تم اقتراح استخدام الهياكل اللولبية المصنوعة بالكامل من السيليكون كمنصة للتطبيقات الإلكترونية فائقة التمدد بسبب المعرفة العميقة لهذه المادة وأدائها العالي. في هذا العمل البحثي أثبتنا استخدام مركب قائم على هيكل لولبي، المستوحى من الهياكل الجزئية للتحسين والحد بشكل كبير من توزيع التوتر و الإجهاد على امتداد الجهاز. وقد تم النظر في دمج اللوالب مزدوجة الذراع مع هياكل مختلفة مثل: هياكل لولبية (ثعبانية) وهياكل حذوة الحصان ، وتم دراسة استجابتها الميكانيكية عند تطبيق تشوه ميكانيكي عليها من خلال تحليل العناصر المحدودة. توفر الهياكل المركبة المقترحة قدرات تمدد ممتازة وتظهر ما يصل إلى 58٪ تخفيض في التوتر / الإجهاد ، فضلاً عن توزيع أكثر اتساقاً بالمقارنة مع التراكيب الأولية الغير محسنة ذات الهيكل اللولبي. وتظهر هذه النتائج الإمكانيات المذهلة للجمع بين الهياكل المختلفة لتحسين سلوكها الميكانيكي، وبالتالي تحقيق منصات أكثر قوة من شأنها دعم تطوير الإلكترونيات القابلة للتمدد. وعلاوة على ذلك، تم أيضاً تصنيع الهياكل المصممة باستخدام تقنيات التصنيع الدقيقة التقليدية للسليكون (100) والسليكون على رقائق العزل (SOI)، على التوالي. وأخيراً تم تعريف الهيكل حلزوني المصنع إلى ما يقرب من 470٪ إجهاد إضافي، لتأكيد فعالية العملية المقترحة

# CHAPTER

## INTRODUCTION

Advancements in bio-integrated systems, wearable technologies, robotics and others, have opened a new era in the field of electronics. This means that new challenges are arising, such as interacting with biology, which is soft, flexible and also stretchable. Therefore, new hybrid electronics devices with electrical properties comparable with the conventional electronics along with advantageous mechanical properties are in need at this time. These desired electronics must have the ability to stretch, flex and bend to a certain radius, depending on the application, along with electrical properties comparable to the present day silicon driven electronics. This new field of electronics, known as flexible electronics, is paving its ways into the electronic industry and has demonstrated a tremendous growth over the last few years. Unfortunately, the conventional and most widely used (silicon based) electronic devices in the current electronic industry lack the above mentioned mechanical properties, although they exhibit outstanding electrical properties and have cost effective manufacturing techniques. As such, even though silicon is the leading material for the manufacturing of these devices, unfortunately it lacks the ability to stretch and bend, thus making the conventional electronics incompatible for the applications where mechanically compliance is also needed.

Researchers are working to overcome the above mentioned issues with the conventional electronics and also finding new ways to achieve electrically as well as mechanically efficient electronic

devices. Several innovative ideas are being engineered ranging from the incorporation of new materials, fabrication of hybrid structures containing polymers, conductors and semiconductors, innovative flexible electronic materials, and novel structures to the conventional electronics. They represent important advancements towards this goal, but there is still a lot to be done and explored. Since, silicon, an inorganic material, is the predominant material in the conventional electronics industry and the processing techniques are very mature and well tested, therefore, a more practical approach towards flexible electronics would be to develop methods and techniques in order to use silicon for flexible electronic devices. Innovative structures, capable of bending and stretching, could provide a mean to achieve stretchable electronics while employing silicon as the main material. The objective of this research work was to improve the understanding of how to use innovative structural modifications in inorganic materials as platforms for flexible and stretchable electronics. It was also the objective to thoroughly study and analyze the compound serpentine-spiral structure and to develop an understanding of how its use can improve the mechanical performance of stretchable electronic devices by compiling, studying and simulating the basic mechanical behavior of a comprehensive set of serpentine-spiral's structures and their potential for actual implementation in flexible and stretchable technologies through the fabrication of those structures. Chapter 2 provides a comprehensive literature review of the current research work being conducted in the field of flexible and stretchable electronics. It also reviews the basic mechanics and parameters usually employed to study the performance of flexible structures. Chapter 3 provides a complete study of the serpentine-spiral structures including the design and simulation of a list of structures. Finally, chapter 4 provides the fabrication flow and explains the fabrication process that was used to fabricate serpentine-spiral structures using bulk silicon(100) and silicon on insulator(SOI) wafers.





# **CHAPTER**

## **LITERATURE REVIEW**

This chapter provides a brief literature review of the current advancements in the area of flexible electronics. Since, flexible electronics differs from the conventional electronics in the sense that it requires a complete characterization of mechanical behavior along with electrical performance. Therefore, this chapter provides a brief review of some of the important mechanical parameters used to study the mechanical behavior of the flexible and stretchable device. It also provides a comparison between main materials (polymers, semiconductors, metals) being used in flexible electronics, in tabular format. This literature review also includes the structures designed in order to provide flexibility as well as stretchability along with their practical applications. Moreover, it also reviews the approaches being researched in order to achieve flexibility and stretchability for electronics devices. These also includes the materials that are naturally flexible and provide a certain degree of conductivity.

### **2.1 Mechanics of Flexible Electronics**

With the continuous advancement of electronic systems, new potential and innovative areas of engineering have emerged to cover an exciting range of novel applications from bio-integrated devices and wearable technologies to smart cybernetics and soft-robotics, or self-powered sensor networks as enablers of the Internet-of-Everything (IoE) and Internet-of-Things (IoT) [1]–[8].

Along with this surge of application areas, electronic systems are being presented with tough challenges in terms of new mechanical requirements and demands. For example, bio-integrated devices and wearable electronics, which deal with complex, mobile, soft, flexible and stretchable biological systems, demand the devices to be conformal to irregular surfaces and to be able to exhibit certain degree of flexibility and stretchability while retaining the high electrical performance of conventional electronics, thus still enabling fast and efficient processing of high amount of information [9]–[11]. Unluckily, conventional electronics, mostly based on silicon, are rigid and brittle in nature, thus lacking the ability to stretch or flex. This makes conventional electronics inherently incompatible with all these applications where mechanical compliance is not only useful but essential. Research work is underway to overcome such challenges, finding innovative ways to achieve both high electrical and mechanical performance. A number of groundbreaking ideas have been proposed, where two main approaches can be identified; I) the use of unconventional materials with conventional electric designs, or II) use of novel strategies and structures to adapt conventional electronics with new mechanical characteristics [10], [12]–[15].

### **2.1.1 Engineering Stress and Strain**

As discussed earlier, flexible electronics are characterized by electrical as well as mechanical properties. Therefore, to verify the compatibility of any device for flexible electronics, mechanical tests must be performed. Several parameters and tests are used to define and verify the material/device's mechanical properties but before going into the details, several terminologies must be defined.

Stress and strain are the most basic parameters in any mechanical test along with stress-strain curves, which are a graphical representation of the material's mechanical properties. Strain, a unitless quantity, is the ratio of change in the material's dimensions with respect to the original [16].

The engineering strain is shown in equation 2.1, where  $\Delta L$  is the change in the length and  $L$  is the

initial length. Strain can be tensile, compressive or shear in nature. Tensile and compressive strain is the measure of the elongation and compression of the material with respect to some reference respectively, as evident from the equation 2.1 as well. Another measure of the strain is shear strain, which results from the application of two forces, opposite in direction, applied to parallel planes [13]. Shear strain is mathematically explained by equation 2.2. Stress, with same unit as pressure, is the force per unit area [16], see equation 2.3, where  $F$  is the applied force and  $A$  is the cross sectional area. It is also the measure of the internal distribution of the forces. Similar to strain, stress is also distributed in tensile, compressive and shear stress. Usually an external load is the main source of the stress but internal mechanism like variation in composition can also induce stress in the material[13]. Fig. 1 describes above mentioned stress measures. We will use Von Mises stress in this study which is a measure to find out if the structure has started to yield (deform plastically and not elastically) at any point during the loading. Yielding is further explained in the next section.

$$\varepsilon = \Delta L/L \quad (2.1)$$

$$\gamma = \tan \theta \quad (2.2)$$

$$\sigma = F/A \quad (2.3)$$

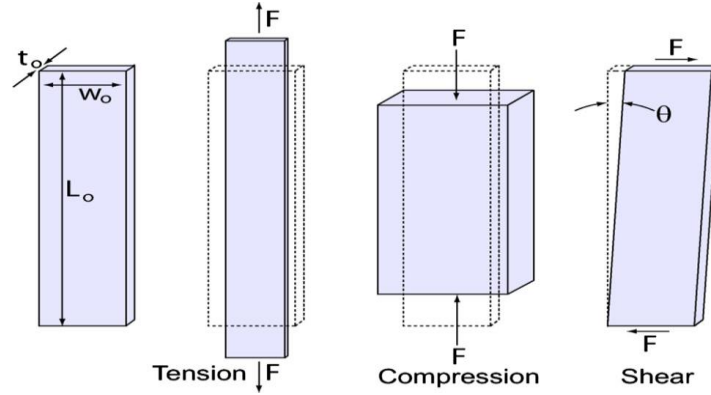


Figure 1 Schematic of measurements of the stress [16]

### 2.1.2 Basic Properties of a Material

Basic properties to characterize the mechanical behavior of materials under stress/strain, include Elastic or Young's modulus, co-efficient of thermal expansion, Poisson's ratio and toughness. Elastic modulus "E", given by equation 2.4, is the ratio of stress to strain in the elastic region represented by the stress-strain curve. The larger the modulus represents stiffer material. Moreover, the stiffness of the material is the function of both, the geometry and the modulus of the material [13].

$$E = \sigma/\varepsilon \quad (2.4)$$

The coefficient of thermal expansion, measured as  $K^{-1}$ , is another very important metric that describes the effect of temperature on the dimensions of the material, because many fabrication processes involve high temperature treatments. Therefore, the prior knowledge of the behavior of the material to the temperature is vital for the manufacturing process as well as for the cost. Another very important metric is Poisson ratio, which describes how a material will be compressed or

stretched in the direction of the applied force. It is the ratio of the transverse strain to the longitudinal strain [13].

### 2.1.3 Toughness

Toughness is the total area under the stress-strain curve. It is the integral of the area under the curve from zero strain to the fracture limit. It is the measure of the resistance of the material under stress or strain, measured in joules per unit volume ( $J/m^3$ ) [13]. Another closely related term is fracture toughness that quantifies the material's ability to resist the crack propagation and brittle fracture. The presence of cracks localizes the stress at the crack tips and this concentration of stress is related to the applied stress by stress intensity factor “ $K$ ” measured in  $MPa\ m^{1/2}$ . At the critical value of  $K$ , which is also the fracture toughness of the material, growth of cracks becomes unstable. Fracture toughness for various types of materials is given in the Fig. 2 [17]. Metals have good fracture toughness and fail by ductile fracture, while oxides, polymers and glass show low fracture toughness [17]. Fig. 2 presents the comparison of fracture toughness between different classes of materials.

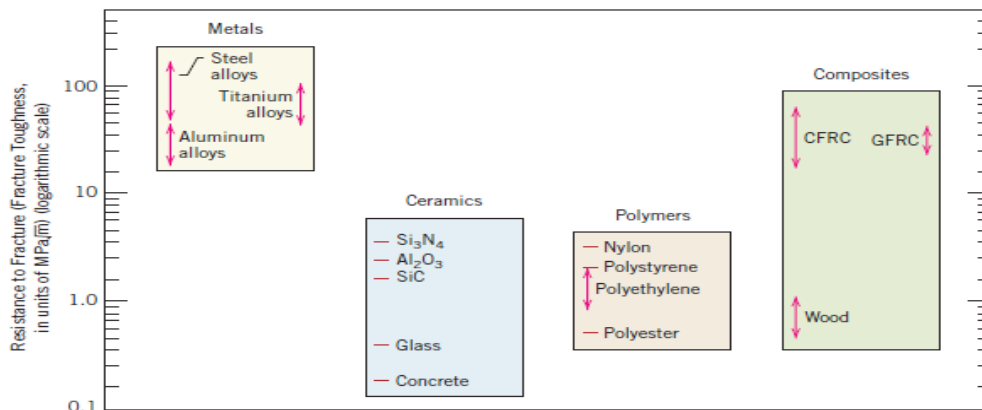


Figure 2 Comparison of fracture toughness between different materials [17]

### 2.1.4 Tensile Test

The tensile test is the most effective tool to study the material's mechanical behavior. In this test, one specimen's end is subjected to uniaxial increasing loading and displacement or elongation is measured as a function of the load. The plot of the stress against the strain results in a curve known as engineering stress and strain curve, as shown in fig. 3. This curve gives a better insight about the material's mechanical properties. The linear region where the stress and strain are proportional is known as the elastic region. Since the material in this region obeys the Hook's law, where the Young's modulus or modulus of the elasticity  $E$  is the constant of proportionality representing the slope of the proportional region of the curve. This represents the ability of the material to return to its original length upon unloading.

The increase in strain may result in deviation from the linear relationship for many materials. The cause of this non-linearity is the internal movement of the atoms or molecules (plastic flow) to achieve equilibrium. The materials lacking this plastic flow are brittle. For example, silicon is a brittle material and lacks the plastic flow property. Therefore, it is not easy to build the flexible electronics with silicon. Therefore, the stress-strain curve for brittle materials typically shows no non-linearity and the material fractures without considerable plastic flow. Moreover, for ductile materials, the stress required to induce strain increases and even after the proportional limit the material shows an increase in strain. This phenomenon is known as strain hardening. The stress at which the material experiences a permanent strain that is not lost even at the removal of the load is known as elastic limit. Moreover, the stress required to induce plastic deformation in the material is known as yield stress. Since the exact value for the beginning of plastic deformation is difficult to identify, therefore, the value of stress that is required to induce the permanent strain of

0.2% is used and known as 0.2% offset yield strength. Another very important term is the maximum yield strength or ultimate tensile strength (UTS), which is the maximum value of the stress the material can withstand and after that point increment in strain requires less value of stress, phenomena known as strain softening. This occurs because after the UTS the cross section of the specimen is considerably reduced so that the engineering stress is much less than the actual or true stress. True stress is given by the equation 2.5 where A is the actual or true area of the specimen. UTS is used for the brittle materials because these materials don't experience the reduction in the cross-sectional area due to plastic flow.

$$\sigma_t = P/A \tag{2.5}$$

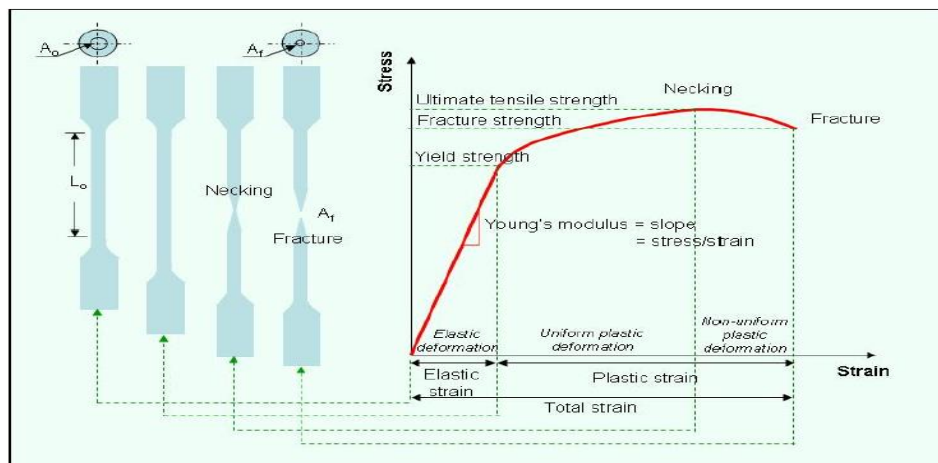


Figure 3 Engineering stress –strain curve for ductile materials [17]

Since the true stress is not uniform throughout the specimen, therefore, some locations will experience more stress and the area at these locations further reduces after the UTS because the localized flow can no longer be compensated by strain hardening. This increase in the local stress increases the localized flow that leads to the neck in the specimen as shown in the Fig. 4. After the



formation of the neck, the stress localizes there and increases until the specimen fractures, a point of failure for the ductile metals. The polymers show different characteristics than the metals. In polymers, the material stretches at the neck to a certain limit, depending on the temperature and specimen processing, and beyond neck propagates to the full length of the specimen. This process is called drawing. Although not all polymers exhibit this property.

### 2.1.5 True Stress-Strain

True stress-strain curve gives more insight to the mechanical properties of the material in the plastic region because the material's dimension undergoes substantial change in this region. Before the occurrence of the neck strain is uniformly distributed in the specimen under tension and during the plastic flow increment in length is compensated by the decrement in the cross-section area of the specimen thus keeping the volume unchanged.

$$dV = 0, \quad AL = A_o L_o \Rightarrow \frac{L}{L_o} = \frac{A}{A_o}$$

where,  $\frac{L}{L_o} = \lambda$  is called extension ratio. True stress-strain can be obtained from the engineering stress-strain curve until necking occurs by the following expression.

$$\sigma_t = \sigma_e(1 + \epsilon_e) = \sigma_e \lambda \quad (2.6)$$

$$\epsilon_t = \ln(1 + \epsilon_e) = \ln \lambda \quad (2.7)$$

If the specimen is subjected to compression the stress-strain curve stretches to the third quadrant. Hysteresis loop can be observed when the specimen is subjected to high cyclic loading to induce

plastic flow between tension and compression and the area of the loop represents the energy released as heat in each cycle per unit volume. In compression, some materials prove to be stronger because of the closing of cracks during compression, unlike tension.

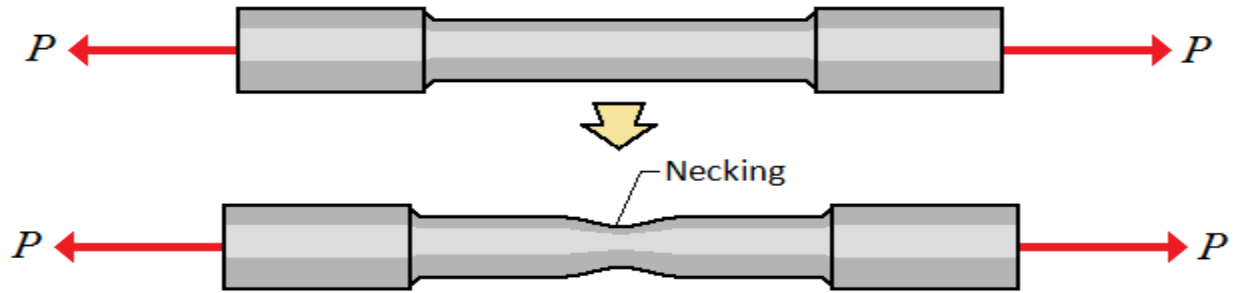


Figure 4 Illustration of necking in Ductile materials [17]

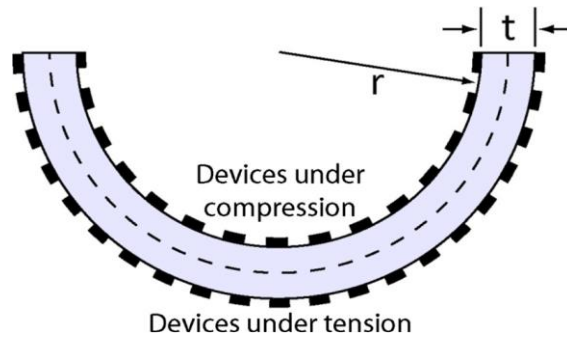


Figure 5 Illustration of a device under tensile and compressive stress and presence of mechanically neutral plane [17]

### 2.1.6 Interaction Between Rigid and Brittle Materials

Bending and stretching are the most common modes for material's deformation. In bending mode, cracking and delamination are the most commonly observed defects and the durability of a flexible device is dependent on the formation and propagation of the cracks and delamination. Cracks are formed and propagate in order to relieve the stress. For brittle materials on flexible substrates first

cracks are formed and then propagates, then their density increases and also the transverse cracks are formed [18]. For brittle materials on flexible substrates, crack formation starts where the substrate's surface is irregular [19] and this is due to the localization of stress at those irregular surface areas [18]. Once cracks are formed they propagate to the entire thickness perpendicular to the direction of the applied strain [18] and continual increase in strain results in denser cracks followed by the transverse cracking and delamination [20]. These cracks also propagate in the substrate catalyzing the device's failure process. Moreover, the mismatch between the mechanical properties of the film and the substrate can result in delamination which in turn leads to failure of the device [21]. The bonding between the substrate and the film can be broken due to the weak adhesion. Also, before delamination, slipping between the materials may occur with increasing strain and cracks are responsible for debonding [21], [22].

In bending mode, the bent sheet undergoes different types of strain. For example, the convex surface experiences tension which might result in cracking while the concave surface, that experiences compression, may lead to debonding from the substrate. Also, in a multi-layered structure, a mechanically neutral plane exists, as shown in Fig. 5 by dotted line, where neither tension nor compressive strain is observed, therefore, positioning the fragile material at the location can improve the mechanical performance of the device. Moreover, if the substrate and overlay layer have the same mechanical properties then the mechanically neutral plane is at the center. This concept of mechanically neutral plane is not valid in the case of stretching mode deformation. In order to devices with several configurations are made to achieve stretchability e.g. the wavy structure that buckled out of the plane as discussed in the structures section.

## 2.1.7 Paths to Flexible Electronics

### 2.1.7.1 Organic/ Polymer Materials

In relation to unconventional materials, organic or polymeric materials are the natural choice due to their excellent mechanical characteristics, giving birth to the notion of flexible, organic electronics, which can provide great flexibility and even stretchability, in contrast to conventionally brittle, inorganic-based devices [10], [23]–[27]. However, their range of applications is, at the moment, limited due to their lower electrical performance, evidently lower compared to silicon, and inability to handle high temperature processing [28]–[30]. The highest hole mobility of  $43\text{cm}^2/\text{Vs}$  for organic thin film transistor was achieved by blended solution of highly aligned meta-stable C8-BTBT and polystyrene using a novel off-center spin coating method [31] which is still very much lower than the silicon. Scalability, on the other hand, is also a very important, merit since the silicon based electronics have reached to ultra large scale integration level which is still very far for organic electronics

Another possible approach is to develop conducting polymers, having the properties of elastomers for mechanical strength combined with other materials for electrical conductivity. This can also resolve the issue of mismatch between the mechanical properties of different interfacing materials in case of hybrid electronic devices. Nanomaterials, due to their excellent electrical and mechanical properties, have drawn the attention of the scientific community. Single nanomaterials can stretch more than the bulk counterpart [23]. Several materials have been used for the fabrication of these films such carbon nanotubes (CNTs), copper nanowires and silver nanotubes [13], [32], [33]. To develop a conductive and stretchable material using nanotubes, the nanomaterials are dispersed on an elastomer like Polydimethylsiloxane (PDMS) [32]. The resulting composite material exploits the electrical properties of the nanomaterials and the mechanical characteristics of the elastomer.

Moreover, due to the presence of redundant paths for the charges, there are less chances for the device to become inactive in case of partial failure.

### **2.1.7.2 Nano Materials**

Carbon nanomaterials derivatives like Carbon black (CB) have been known for their excellent electrical properties and can be used as a filler for elastomers to enhance the electrical and mechanical properties of polymeric materials. Unfortunately, CB is not friendly to the environment and higher fraction of this material is needed to avoid agglomeration and to avoid the obstruction of the conductive path in the composite material [34].

Carbon nanotubes (CNTs) other derivatives are also used to make stretchable conductive composites and proved to be a promising material because of its mechanical properties required for flexible electronics. This ecofriendly material, when used as a filler improves both electrical and mechanical properties of the polymer [31], [35], [36]. Also, these properties are controllable by changing the percentage of Single wall carbon nanotubes (SWCNTs). For example, n and p channel transistor formed using the perfectly aligned linear array of single-walled carbon nanotubes (SWCNTs) demonstrated mobilities of approximately  $1000 \text{ cm}^2/\text{Vs}$  [37]. The main issues related to the CNTs technology included the electrical properties dependency on the dimension and structure of single walled carbon nanotubes (SWCNTs), high resistance and low currents in networks and composites and achieving the adequate assembly of SWCNTs required to build circuits[38]. Although, the results using SWCNTs are encouraging but still they are far behind than the current silicon based electronics in terms of integration density and computational power. Graphene, a two-dimensional (2D) sheet of covalently bonded carbon atoms, is also being used in flexible electronics due to its exceptional properties (Fig. 6). Electrical and mechanical properties can be improved by fabrication of composite materials by mixing Graphene with Polymers, metals, oxides,

etc [39]. Finally, nanoscale metals also exhibit flexibility and can be used as flexible conductors. For example, Ag nanowires can be used as conductors but have large sheet resistance. Several techniques have been studied to lower this resistance [40]. Cu and Au nanowires were also studied for flexible applications. Cu nanowires are very good conductors and are flexible too, although they are not stable in air and therefore they require a Ni protective layer at the expense of conductivity. The overall performance of Au and Cu is lower than Ag. A comparison between different metal nanowires is presented in [40].

As mentioned earlier, electronics has three main building blocks: conductors, semiconductors, and insulators. Each of these components has their part towards the device functionality but semiconductor is the most important one. Starting from the conductors, metals are the best-known conductors with conductivity ranging from  $\sim 10^4$  to  $10^6$   $S/cm$ . Moreover, thin sheets of metals are capable of handling a moderate amount of strain. We know from  $\varepsilon = t_s/2R$  that the strain and radius of curvature can be used to describe the bendability of a bar, where  $\varepsilon$  is the strain,  $t_s$  is the thickness and  $R$  is the radius of curvature[28]. Several metals have been used in flexible electronics like Ti/Au or Ti/Pd. In [41] Ti/Au (5/30 nm) and Ti/Pd (0.5/35 nm) were used as back-gate in thin-film transistors consisting of semiconducting CNT networks. The resulting integrated circuit was tested for bendability by wrapping it on a metal rod of 2.5 mm in diameter. Unfortunately, in applications requiring higher strains, metal film didn't provide promising results thus forcing the researchers to look for other materials to replace metals in flexible electronics. Other materials are supposed to have electrical properties comparable to the metals. For example, in [42] ultra-stretchable fibers filled with metal alloy of eutectic gallium indium (EGaIn) injected into the hollow elastomeric fibers are proposed. The alloy is liquid at room temperature and the overall structure, along with good electrical properties, exhibited the ability to withstand higher deformations.

Nevertheless, encapsulation is required to avoid liquid leakage, as well as complex fabrication techniques[13].

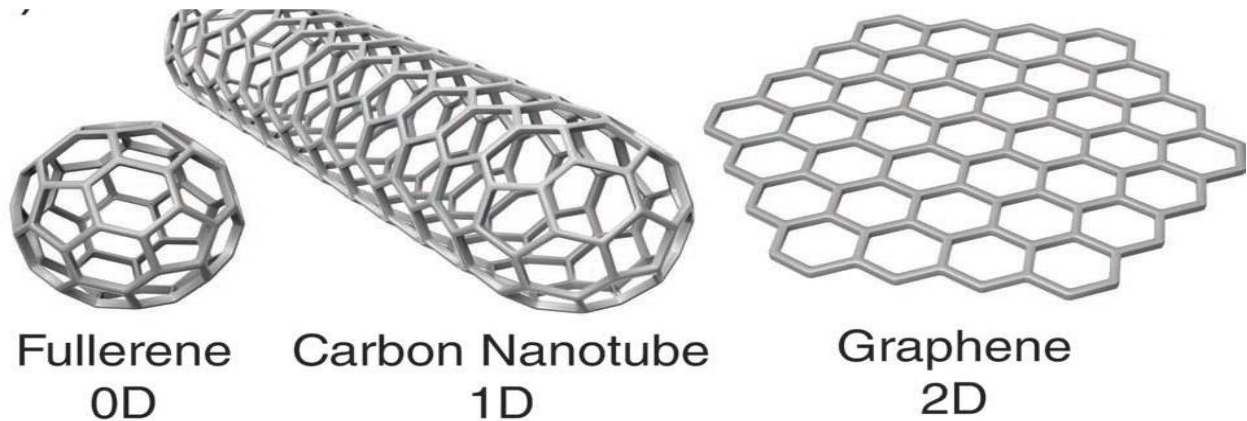


Figure 6 Allotropes of carbon, two-dimensional graphene (right), quasi-zero-dimensional buck-minsterfullerene (left), and quasi-one-dimensional armchair nanotube (middle) [39]

### 2.1.7.3 Conducting Oxides

Transparent conducting oxides (TCO) are also being used as conducting connectors in flexible displays. Indium tin oxide (ITO), the most dominant in optoelectronics due to its transparency and conductivity, is the most prominent conducting oxide. The conducting oxide can be deposited on a flexible substrate but mismatch in the mechanical properties of the flexible substrate and ITO remains a challenge since the conducting oxide may break during fabrication or crack during use. For example, ITO was used as the gate terminal and was tested to radius of different curvatures till 0.4cm in [37], but at higher strain device failure occurred due to fracture in the gate electrode (made of ITO). Therefore, conducting oxide (ITO), although very transparent and conducting, cannot be used as a flexible conductor due to lack of mechanical compliance in applications with higher strain and cyclic loading.

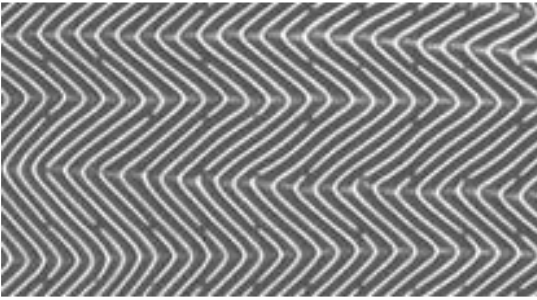
Since, flexible electronics is a combination of metals/conductors, semiconductors and polymers. And unfortunately, these materials have different properties because they don't belong to the same group of materials. Their interaction in a device is also a challenge because of their poor interaction with each other. Therefore, it is very important to choose a set of these material for the optimum performance. For example, polymers with higher melting point must be used when the fabrication process involves higher thermal budget process. In table.1 and table.2 we provided a comprehensive catalog of the materials being used in flexible electronics with the values of their most important parameters. It is evident from the table that polymers have much lower melting point and electrical conductivity as compared to metals and silicon. Whereas mechanical strength of metal/ silicon is far below the polymers. Therefore, to have a flexible device, a combination of polymers and metals/semiconductor is vital. Polymers provide better mechanical support while the semiconductor/ metals exhibit a better electrical performance.

### **2.1.8 Structures**

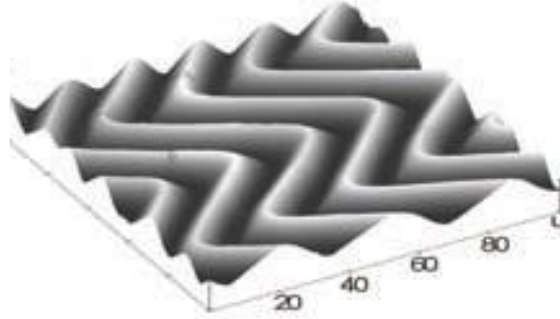
A key aspect in electronics is integrating three different materials to build a practical device. These materials are conductors, insulators, and semiconductors. These materials vary from each both electrically and mechanically. The organization of these materials in flexible electronics is also a major challenge since the strain demands of each of these class of materials is different. Different approaches have been employed for their integration and organization. The most effective approach is the arrangement of brittle and rigid materials on flexible substrates like elastomers. Unfortunately, this technique also suffers from different modes of failures like, slipping that can occur between the layers of different materials, cracking upon bending can also result in device's failure and even delamination can also occur upon bending due to bad adhesion between the layers [43]. Generally, there are two main approaches employed for the design of flexible and stretchable electronics, 1) new structures for conventional electronics 2) new materials with the conventional structure [10]. The first approach exploits the fact that ultra-thin rigid materials become flexible



and able to bend to a certain radius [29]. For example, silicon which is brittle and rigid in nature becomes flexible when its thickness is reduced to micro- or nanoscale [28] [10]. Therefore, making the devices with ultra-thin silicon sheets can give flexibility to a certain level. Furthermore, some structural changes to the thin membrane can improve the mechanical performance of the structure. For example, a wavy silicon structure transferred onto PDMS is shown in Fig. 7 [44], [45]. By transferring silicon nanomebranes onto polymeric substrates, mechanical stress can be highly reduced in the structure, while maintaining the excellent electrical properties of silicon. In [46] an array of nanoribbons (NRs) were transferred onto a pre-strained PDMS After the pre-strain is remove, the PDMS shrinks down to its original size and the nanoribbons rise as shown in Fig. 8. There is no actual bonding between the non-coplanar silicon nanoribbons and the elastomer so they can easily rise. The wavy shape of the structure provided the end to end stretchability and offer elastic response when the strain is applied to the structure [43], [47]–[50]. For encapsulation and protection purposes, a top layer of PDMS can also be coated. Moreover, locating the silicon sheet towards the neutral mechanical plane of the structure can improve the performance by reducing the strain on the mechanically less elastic silicon sheet [43]. A similar strategy is applied by replacing the straight NRs with serpentine traces. In this case the level of stretchability is further improved because higher elongation can be reached by buckling induced, twisting deformation and sequential unfolding of the serpentine structures [46].

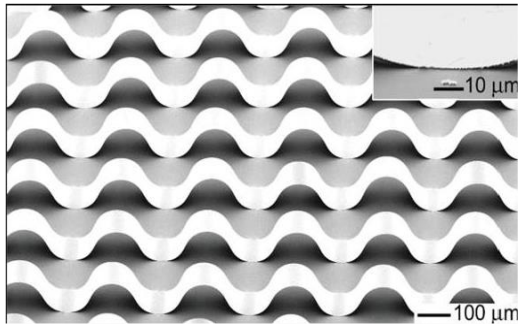


(a)

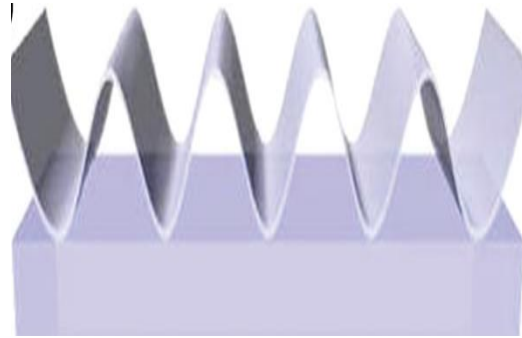


(b)

Figure 7 (a) Silicon membrane in wavy structure ( $\sim 100$ -nm thickness), (b) wavy shape silicon bonded on an elastomer [10]

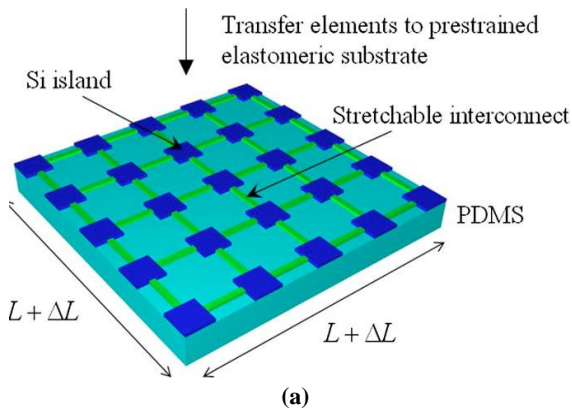


(a)

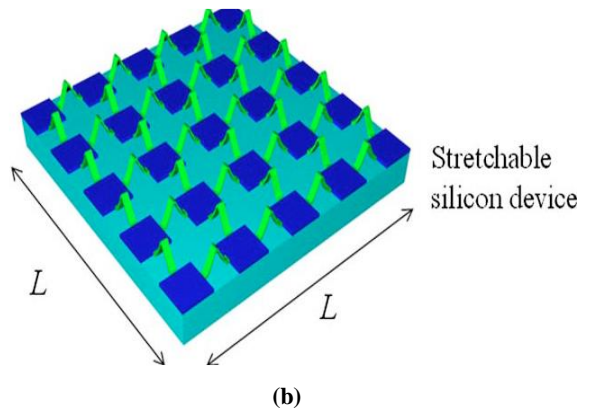


(b)

Figure 8 (a) Array of silicon NRs in wavy configuration (b) schematic of 1D Buckled NRs bonded on elastomer at troughs [47]



(a)



(b)

Figure 9 (a) General illustration of the flexible electronics in mesh structure in stretched form and (b) un-stretched form [55]

### 2.1.8.1 Islands Interconnect Approach

An immediate extension to these strategies consist in arranging the brittle semiconducting materials, containing the active electronics, in arrays of rigid islands, as shown in the Fig. 9, which are spatially distributed over an elastic substrate and electrically joined through especially designed metallic interconnects [51]–[56]. The design of these interconnects is prepared in a way that the structure is able to mitigate strain induced during the flexing, bending, stretching or even twisting. The main idea behind this arrangement is to minimize the stress localization at the brittle components of the electronics[13]. Another benefit of this scheme is that it provides the freedom to separate and reorganize the different components of the system such as power management, sensor modules, communication, etc. Unlike the islands these interconnects can be stretched due to their structure. Several approaches have been proposed for these interconnects. Designing interconnects into stretchable forms can result into a structure able to withstand large strain deformations.

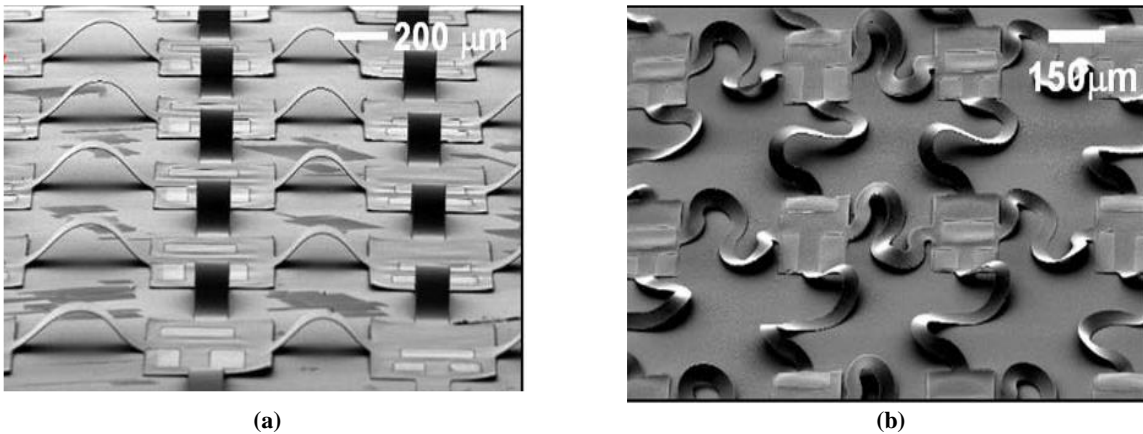


Figure 10 (a) Non-coplanar mesh design on elastomer (b) mesh serpentine structure under strain [15]

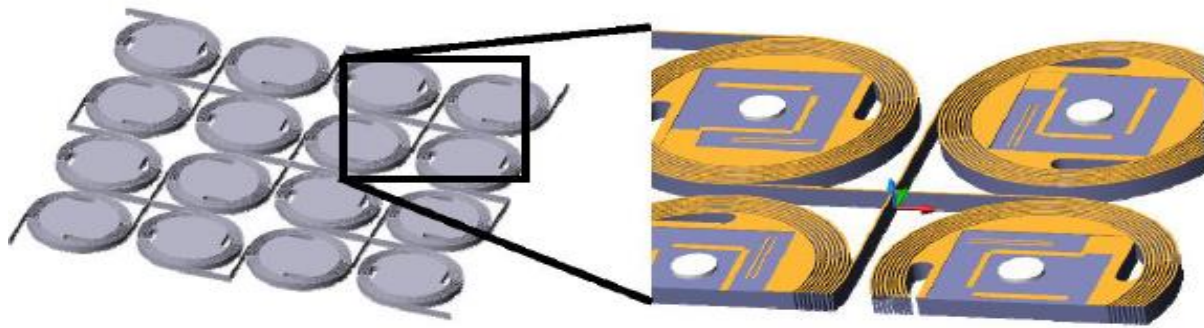


Figure 11 Schematic of 2D network of silicon Islands with spring spiral interconnects [62]

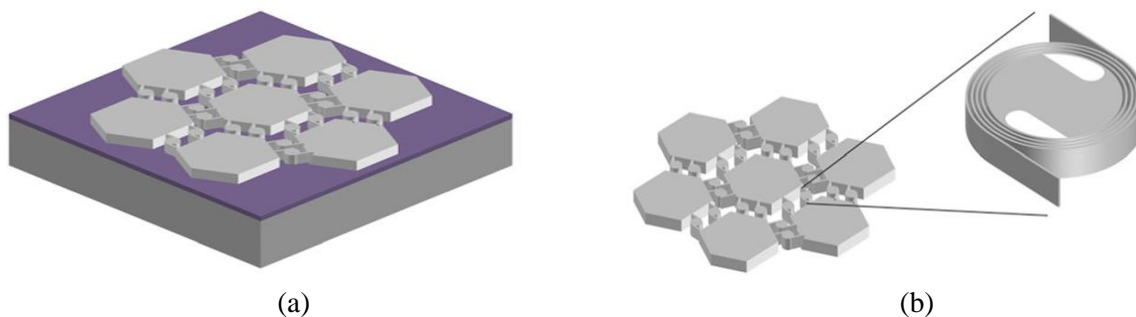


Figure 12 (a) hexagonal islands with spring spiral interconnect (b) the spiral interconnect between the islands [28]

Unlike the islands, interconnects can be stretched due to their structure. Designing interconnects into stretchable forms can result in structures that can withstand large strain deformations. Kim *et al.* [57] developed a concept to build a network of islands on an elastomer and then connecting the islands through buckled-arch shaped interconnects as shown in the Fig.10a. Upon the application of applied strain, interconnects move out of the plane to mitigate the effect of the applied pressure. In the same work, an alternative structure was also proposed by replacing the straight-arch-shaped, buckled interconnects with effectively longer serpentine bridges such that the effect of external strain is compensated by the change in height and geometry of non-coplanar serpentine, shown in the Fig.10b. The effect of external strain is compensated by the change in height and geometry

of non-coplanar serpentine. Moreover, the peak strain experienced by the metal layer in the serpentine bridges and islands was reduced to as low as 0.2% and 0.5% when 70% of stretching strain was applied.

### **2.1.8.2 Fractals**

A powerful alternative configuration comes from naturally occurring structures known as fractals, a self-repeating structure that can provide stretchability to a larger extent. The use of fractal structures, such as Peano, Greek cross or Vicsek, for stretchable electronics was demonstrated by Fan *et al.* [58] in a health monitoring and communication application. It also showed that higher order fractal structures demonstrate better stretchability; for example, third order Peano layout showed more than 20% stretchability, which is even higher than skin's elastic limit. Recently, Yan *et al.* [59] developed a novel technique to build complex 3D out-of-plane topologies using multilayer 2D precursors on a pre-strained substrate, studying the use of a variety of geometries, such as circular cages, blooming flower, entangled wavy arcs, etc., with the potential for innovative out-of-plane, stretchable applications, like a demonstrated spiral-based tunable inductor for wireless communication. Similarly by using compressive buckling Xu *et al.* [60] demonstrated to transform 2D structures into 3D. Several 3D geometries were studied that resulted from their 2D precursors like Helix, toroids and spirals.

The use of spiral structures is of especial interest for us due to their advantageous mechanical characteristics. For instance, it has been recently demonstrated by Lv *et al.* [61] that spiral-based structures can provide larger stretchability as compared to serpentine-based structures with the same in-plane area (plastic deformation reached at ~100% applied strain with serpentine-based structures, compared to 200% for the spiral). In fact, the use of spirals as ultra-stretchable interconnects has been already proposed by Huang *et al.* [62] earlier on, where a topology of silicon-

based circular islands, meant to host electronics, were physically interconnected through silicon spiral springs in a 2D network, shown in Fig. 11. In this work, a very large area expansion ratio of 51 times the original size was achieved, which can be extremely advantageous in macro-electronics applications. Expanding on this, it has been demonstrated that the stretchability ratio can be even further improved by increasing the number of the spiral springs in an area-efficient way. Thus, an all silicon-based network with hexagonal islands was proposed, where the islands were physically interconnected with double-arm spiral structures, such as the one shown in Fig. 12, reaching an unprecedented stretchability of more than 1000%. Additionally, the base of spring arms were modified with serpentine-like structures to mitigate the effect of high strain at both ends, thus reducing the localized strain at these points by half and evenly distributing it throughout the spiral structure [28]. Practical implementations that use spiral structures to build highly stretchable systems for diverse applications have been demonstrated as well. For instance, Mamidanna *et al.* [63] demonstrated the excellent mechanic and electric performance of spiral-shaped, reactive ink-based interconnects, showing outstanding stretchability (160% to 180%) with only ~2.5% variation in electrical resistance after being subjected to 1000 elongation cycles. More recently, a spiral-inspired stretchable thermoelectric generator (TEG) was shown to, interestingly, generate higher electric power while being stretched. This can be easily explained since the temperature gradient increases at stretching, given the adequate conditions [64]. Several other applications make use of serpentine structure in flexible electronics [65] and others have used planar mesh structures with “S” shaped interconnects between the islands as shown in fig. 13 [66].

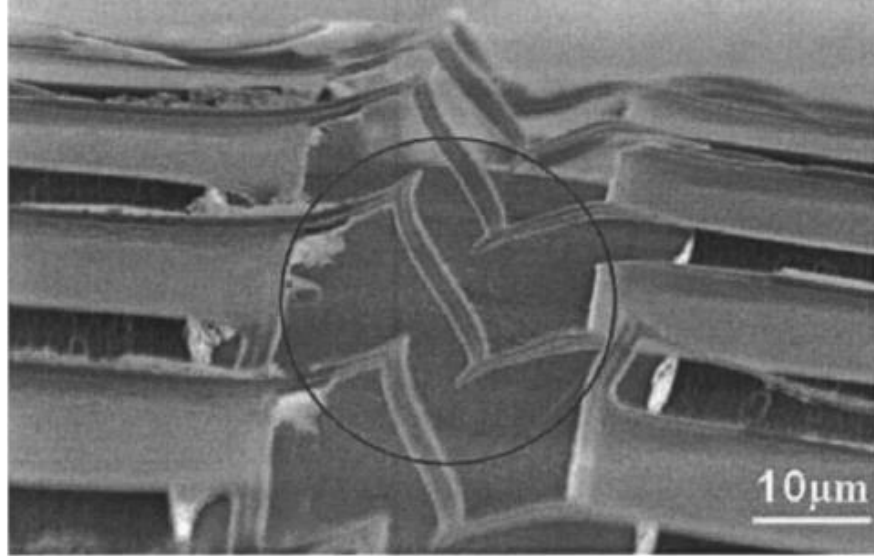


Figure 13 S-shaped micro-fabricated suspensions when no pressure was applied to the membrane [66]

### 2.1.9 Thin Films

Different methods and approaches have been employed to achieve the flexibility/stretchability in electronic devices. These efforts not only include the development of new techniques for making the flexible materials conductive but also developing new methods to make the conductive materials flexible. Since flexural rigidity is a function of thickness of the materials as represented by the equation. 2.8, this shows that flexibility can be increased by decreasing the thickness of the material [67].

$$D = \frac{Et^3}{12(1-\nu^2)} \quad (2.8)$$

Silicon is the flagship material in semiconductor industry and it has very mature fabrication processes over many years, therefore, it is desirable to make flexible devices using this material. Several efforts have been made by using the silicon in hybrid devices with polymers. This is one

possible way to combine the excellent electrical properties of silicon and mechanical properties of polymers to achieve the desired results. Micro-structured silicon can be released from silicon-on-insulator (SOI) wafers, and then transferred onto polymeric materials, like Polyimide (PI), PDMS or Polyethylene terephthalate (PET), using a transfer printing technology and finally, circuits can be built on the polymeric sheet [68]–[72]. Unfortunately, despite having the capability of achieving high device's complexity using this technique, the polymers are incompatible with the high thermal budget processes required to fabricate complementary metal oxide semiconductor (CMOS) devices as polymers are not capable of handling such high temperatures. An alternative method employs the technique of thinning the silicon. In this method, devices are first fabricated on the silicon wafer and then using thinning technologies, like grinding or polishing the backside of silicon substrate, to thin down the substrate and thus achieve flexible devices. However, grinding the back of the silicon to few micrometer wastes a large part of the wafer. Moreover, thinning the wafer to a thickness required to achieve flexibility might damage the substrate itself and induce non-uniformity, which might result in a defective device [73]. Another technique to produce thin substrates employs the stresses to fracture the substrate at the specific depth. Stress is exerted through the deposition of nickel on the passivated devices, which leads to fracture at a specific depth depending on the amount of stress. Finally, a thin layer can be peeled off from the wafer [74]. Nevertheless, the ultra-thin body silicon on insulator (UTB-SOI) used to demonstrate this technique, although it resulted into a very thin and high performance flexible platform, it is a very costly substrate, representing a major drawback of this technique. An additional technique consists of a two-step anodic etching producing a double layer porous silicon to be formed. Next, through a high thermal budget process the lower and less dense layer is removed and a porous silicon membrane hanging on the substrate is achieved. Finally, a silicon layer is epitaxially grown on the



hanging silicon membrane, on top of which the electronic devices can be fabricated. Again however, complex and expensive processes might hinder the implementation of this method [73]. Another very simple technique was presented by Rojas *et.al* [75] to produce an semi-transparent, porous, and mechanically flexible thin film using a cheap mono- crystalline silicon (100) substrate [76]–[78]. This technique employs sequential anisotropic and isotropic etching processes to peel off a very thin layer of silicon from the wafer, shown in Fig. 14. Moreover, the rest of the wafer can be reused, thus making the process very cost effective. Similarly, in another technique presented by Rojas *et.al* [28], the author presents a very simple 5 step process to fabricate an all-silicon based flexible and ultra-stretchable structure using a SOI wafer and conventional micro-fabrication techniques. Stretchability was achieved thanks to the use of double-arm spiral structures, which can reach very high stretch ratios while un-wrapping. The spirals were used to interconnect bigger “islands” where the electronic devices can be fabricated. Although, the SOI is comparatively expensive, the simplicity of the process is favorable for the fabrication of mechanically flexible devices. Fig. 15 shows the 5 steps involved in the process.

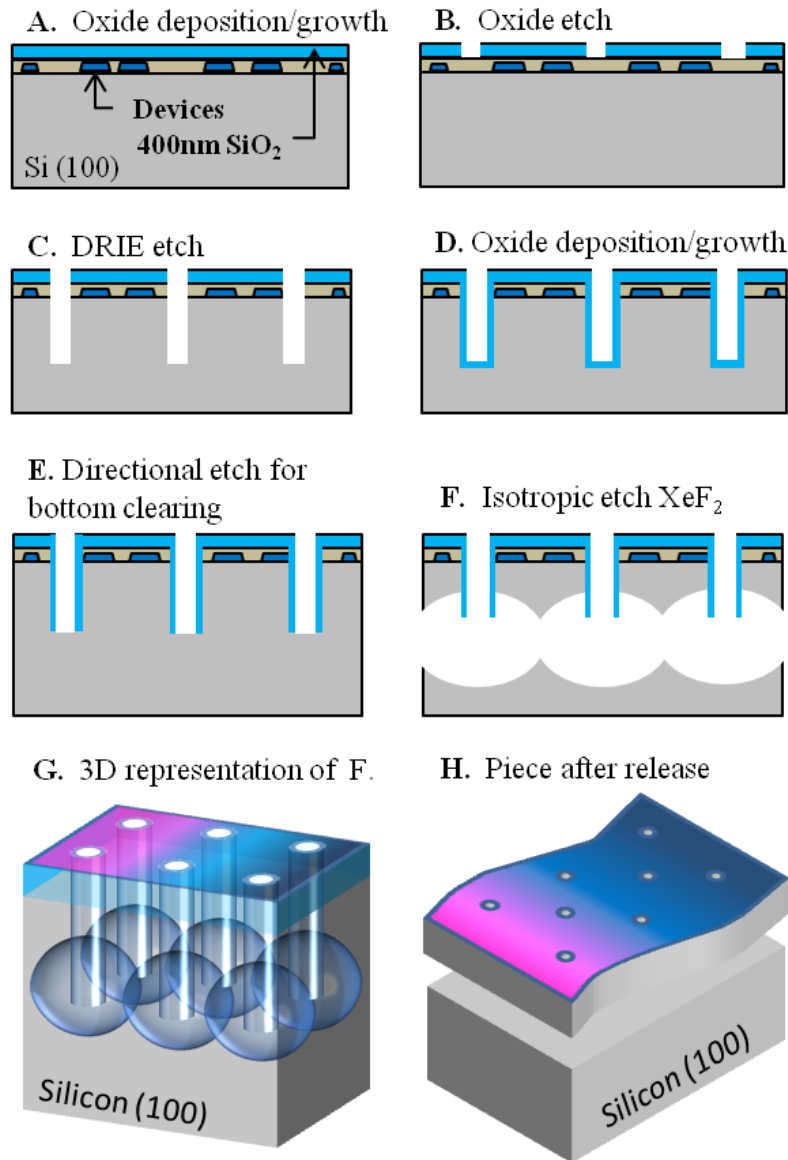
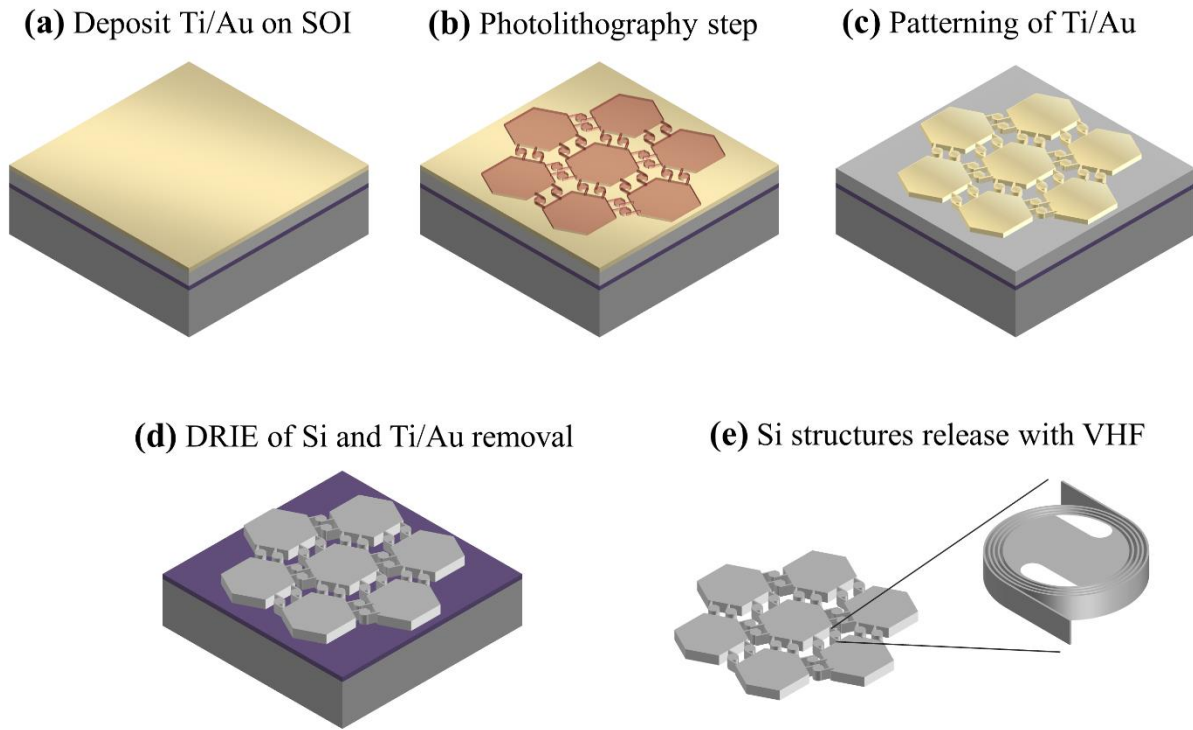


Figure 14 Fabrication process flow for releasing silicon pieces from mono-crystalline silicon wafer [75]



**Figure 15 Fabrication process flow for releasing double arm spiral structure from SOI wafer [28].**

Inspired by these all-silicon, spiral-based structures and by the concept of fractals, in this study we will analyze the effect of replacing the straight arms of the spiral with serpentine arms along with modifying the inner structure. The analysis will be carried out through finite element analysis (FEA), Moreover the effect of replacing the spiral's arms with serpentine and horseshoe structures for maximum stress and strain reduction, while maintaining an efficient use of area will also be studied. This fractal-inspired concept, although not self-repeating, consists of the effective combined use of spiral, serpentine and horseshoe structures (a structure within a structure). Further, the fabrication of the proposed structures will be carried out using standard microfabrication techniques.

**Table 1 Main properties of common polymers.**

Properties	Polymeric Materials			
	PMMA	PDMS	PET	PI
Mass density	1170 - 1200 kg/m <sup>3</sup>	0.97 kg/m <sup>3</sup>	1290 - 1400 kg/m <sup>3</sup>	1.42 g/cm <sup>3</sup>
Young's modulus	1800 - 3100 (Mpa)	360-870 KPa	2.76 - 4.14 Gpa	2.0-3.0 Gpa
Poisson ratio	0.35-0.4	0.5	0.37-0.44	0.34 @ 23°C
Tensile or fracture strength	48-76 MPa	2.24 MPa	48.3 - 72.4 Mpa	70-150 Mpa
Specific heat	1466 J/kg.K	1.46 kJ/kg.K	1.20 - 1.35 kJ/kg.K	1090 J/kg.K
Thermal conductivity	0.167-0.25 W/m.K	0.15 W/m K	0.15-0.4 W/m K	0.10-0.35 W/m.K
Dielectric constant	2.6 at 1MHz	2.3-2.8	3	3.4
Index of refraction	1.492	1.4	1.58-1.64	1.7
Electrical conductivity	10 <sup>14</sup> - 10 <sup>15</sup> Ω.cm	4x10 <sup>13</sup> Ω.m	10 <sup>16</sup> Ω.cm	1.5x10 <sup>17</sup> Ω.cm
Magnetic permeability		0.6x10 <sup>6</sup> cm <sup>3</sup> /g		
Melting Point	130°C	-49.9–40°	250-260 °C	no melting, Decomposes at 520°C
Coefficient of Thermal Expansion	70-77 x10 <sup>-6</sup> K-1	310x10 <sup>-6</sup> /C	20-80 ( x10 <sup>-6</sup> /K)	30-60 ( x10 <sup>-6</sup> /K )
Water absorption, 24 hours	0.3 -0.4 %	>1%	0.10%	0.2-2.9 %
Glass transition temperature	105°C	150 °C	60-80 °C	

**Table 2 Main properties of common conductors and semiconductors**

Properties	Materials			
	Aluminum	Copper	Silicon	Germanium
Mass density	2712 kg/m <sup>3</sup>	8940 kg/m <sup>3</sup>	2330 kg/m <sup>3</sup>	5.323g/cm <sup>3</sup>
Young's modulus	70 Gpa	130 Gpa	165 Gpa	130GPa
Poisson ratio	0.33	0.34	0.27	0.3
Tensile or fracture strength	40-50 Mpa	193-262 Mpa		135-150 Mpa
Specific heat	0.91 KJ/kg.K	385 J/kg.K (300 K)	0.71 KJ/kg.K	321 J/Kg.K
Thermal conductivity	237 W/m-K	401 W/m-K (300K)	1.56 W/cm-K	64 W/m-K
Dielectric constant	1.6 - 1.8	6.0 - 6.2	11.68	16
Index of refraction	1.44		3.42	4.064
Electrical conductivity	$3.2 \times 10^{-8} \Omega \cdot m$	$1.7 \times 10^{-8} \Omega \cdot m$	$2.3 \times 10^3 \Omega \cdot m$ (20 °C)	0.5 $\Omega \cdot m$
Magnetic permeability				
Melting Point	660.3 °C	1,085 °C	1,410°C	938.25°C
Coefficient of Thermal Expansion	22.2 ( $\times 10^{-6} /K$ )	16.6 ( $\times 10^{-6} /K$ )	$2.63 \times 10^{-6} K^{-1}$	$5.9 \times 10^{-6} C^{-1}$

## CHAPTER

# RESULTS AND DISCUSSION<sup>1</sup>

This chapter contains the information about the design and simulation of the structures designed for stretchable and flexible electronics. It also provides a brief review of the mechanics of the geometries of the structures involved in the study. Moreover, the simulation workflow will explain the simulation environment that was used in order to study the mechanical behavior of each structure along with the parameters required for study. Several structures were designed in order to achieve the desired mechanical performance, required for devices that demand flexibility as well as stretchability. The structure design was a step by step process and based on the observations at each step, improvements were made in the next step in order to remove those short comings. Therefore, several geometrical designs were used in one compound structure, combining the spirals with serpentes and horseshoes, in order to remove the shortcomings of the single geometrical design. Each structure was simulated for two very important mechanical parameters, stress and strain, and the distribution of those parameters along the structure was studied to find the areas where improvements were necessary along with noting the maximum values localized at those points. Then efforts were made to decrease the stress localization at the critical areas in the structure. The mechanical performance of each proposed structure was evaluated and compared with the spiral based structure.

---

<sup>1</sup> © 2017 Elsevier Ltd. Reprinted, with permission, from Mutee U. Rehman, Jhonathan P. Rojas in *Optimization of compound serpentine-spiral Structure for ultra-stretchable electronics*, *Extreme Mechanics Letters* 2017, 15, 44–50.

### 3.1 Simulation Workflow

In general, serpentine/horseshoe structures contain periodic cells; one unit cell with equal halves with each unit cell containing two half circles of radius  $R$ , thickness  $t$ , arch angle  $\alpha$ , width  $w$ ,  $S$  is the end-to-end distance and length  $l$  between the half circles (reference schematic can be seen at the inset of Fig. 27(a)). The analytical solution of the in-plane serpentine/horseshoe mechanic behavior has been studied in detail in previous works [79]–[81].

The general equation for end-to-end distance,  $S$ , in case of horseshoe serpentine structure, presented in [79], is given as,

$$S = 4 \left( R \cos \alpha - \frac{l}{2} \sin \alpha \right) \quad (3.1)$$

The above equation shows that for higher stretchability, the radius  $R$  of the half-circle plays a vital role and is directly proportional to the end-to-end displacement, whereas the thickness  $t$  of the structure will have no effect.

Additionally, a useful non-linear theoretical model for fractal-inspired horseshoe microstructures has been already developed by Ma *et al.*[82], which also demonstrated that by increasing the order of the horseshoe, the stretchability of the system would be improved. In our case, we are interested in the incorporation of serpentine structures, with  $\alpha = l = 0$ , within the spiral design in order to have a simpler design with less area usage. Later on, we also incorporated horseshoe structures to minimize stress and strain in specific areas only. Although horseshoe structures might provide better stretchability and less stress localization, we used them partially in our structure mainly because they take up more space than a simple serpentine, especially if we consider the use of several turns around the spiral to maximize the stretchability, without utilizing too much area.

The maximum strain in the case of the spiral structure is given as [28]:

$$\varepsilon_{max} = \frac{w}{2R_S - w} \quad (3.2)$$

where  $R_S$  is the radius of the inner circle of the spiral (Fig. 1(a)), and  $w$  is the width of the arms. Similarly, the maximum strain in the case of the serpentine, with  $\alpha = l = 0$ , can be expressed as [45]:

$$\varepsilon_{max} = \frac{6w}{R - w} \quad (3.3)$$

where  $R$  is the radius of the inner half-circle in the serpentine, and  $w$  is the width of the arm, see Fig. 9(a).

Both the above equations (3.2 and 3.3) show that the maximum strain is directly proportional to the width and inversely proportional to the radius of the half-circle. Consequently, the design should try to maximize the radius to width ratio of both structures, bearing in mind area and fabrication constraints. In the case of the spiral, we chose a width of 5  $\mu\text{m}$  and the radius of 250  $\mu\text{m}$ , such that the strain reaches to a maximum of 1%. For the case of the serpentine the width remains the same (5  $\mu\text{m}$ ) and the radius  $R$  of each half-circle was selected to be 14.5  $\mu\text{m}$ , mainly considering an adequate spacing between the spiral's inner circle (250  $\mu\text{m}$ ) and serpentine's half-circle (trough of the serpentine). In addition, the maximum stretchability achievable using the spiral structure with two arms is dependent on the number of turns in the spiral. This is shown by the equation below.

$$E_{max} = 2\pi N \quad (3.4)$$

where  $E_{max}$  and  $N$  represent the maximum stretchability achievable and number of turns of the arms respectively. Equation 3.4 is a simplified expression, which shows us that the main parameter for reaching a specific stretchability is simply the number of turns  $N$ .



We studied several variants of the serpentine/horseshoe structures and their mechanical response was analyzed through finite element simulations. At first, by replacing the spiral's arms with serpentine structures the stress and strain distribution was analyzed to identify weak areas. Subsequently, the arms' structure was further optimized, where the main objective was to not only reduce the strain but also to minimize the stress localization near the critical areas; the starting and the ending of spiral's arms. Finally, optimized serpentine-spiral structures were analyzed and their performance was compared with the original spiral-based structure. To carry out the finite element simulations COMSOL Multiphysics was used. 2D geometries, designed in SOLIDWORKS, were imported into COMSOL Multiphysics using its CAD import tool and then extruded to 3D at a height of 50  $\mu\text{m}$  (thickness of thin-silicon substrate). The geometry was partitioned into different domains for better mesh distribution efficiency. The top surface of the inner circle was used to create a coarse quad-based mesh, while the arms were used to create finer triangular-based mesh for highest detail. Using the sweep function, the top layer meshes were propagated to the whole geometry. For boundary conditions, one arm was kept fixed while the other was subjected to a prescribed displacement, as shown in Fig. 3(a), and the stress and strain values were analyzed at a maximum displacement of 1.8 mm, reached in gradual steps of 50  $\mu\text{m}$ . We also included the effect of geometric non-linearity due to the large deformation of the structure. Finally, silicon (single-crystal isotropic) was used from the material library.

## **3.2 Simulation Environment**

As mentioned earlier, this research work explored the possibility of finding new structures in order to enhance the mechanical performance by removing the constraints found in the previous structures. In order to achieve that we proposed a compound structure that contains both the spiral and

serpentine. First of all, a simple spiral based 2D structure with two arms was drawn and then imported to COMSOL MultiPhysics using its CAD import tools and then extruded to 3D. Isotropic Silicon was used as the material for the whole structure. Since the spiral's inner circle was just a simple plane therefore, we selected a normal mesh in order to reduce the number of elements whereas the arms were meshed with extra fine mesh because of their width and symmetry. The extruded geometry, shown in Fig.16(a), was then simulated in order to analyze the stress and strain distribution along the arms and also to identify the areas with maximum stress and deformation. To carry out the finite element simulations, the end of one arm was fixed and other arm was subjected to a prescribed displacement and the stress and strain values were analyzed at 0.0018m.

### **3.2.1 Standard Spiral Structure**

The maximum stress, at the end of the spiral arm under displacement, was 8698 MPa, as a result to the prescribed displacement. Similarly, the percentage peak strain was about 4.23%. The stress and strain distribution along the arms is shown in Fig.16(b), Fig.16(c) The value of both the stress as well as strain is high at the end points as shown in Fig.16(d), Fig.16(e). Since the end points can be connected to another island therefore, it is vital that this point must have a lower stress/strain localization and also the arms should have a uniform stress distribution. To reduce the stress at the end we added a triangular end as shown in Fig. 17(a). This end structure provides a smoother transition from the thin spiral arms to the next island to which the arm is to be connected. The simulation results for stress and strain, in Fig. 17(b), Fig. 17(c), Fig. 17(d), Fig. 17(e), revealed that the maximum stress as well as strain decreased considerably by adding triangular like ends as compared to the spiral without end structures. The peak stress was found to be at 4824 MPa which is almost half of the one found in case of spiral without end structures. Similarly, the percentage

strain also reduced to 1.49%. These results show that the addition of end structure at the end of the arms results into the reduction of the stress and strain localization.

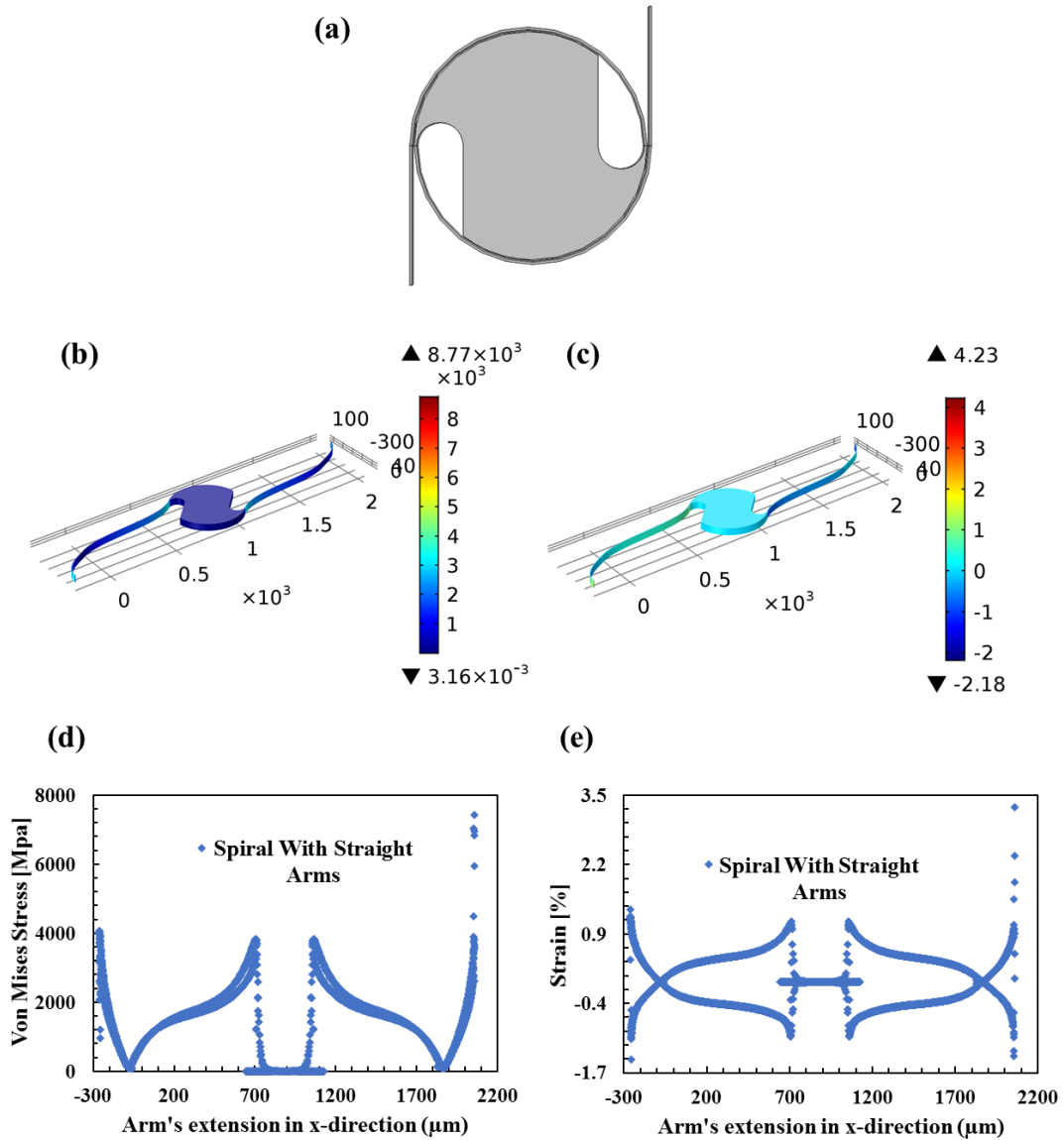


Figure 16 Spiral Structures with straight arms (a) spiral structure with two arms, (b) stress distribution along the arms (c) stress distribution along the arms (d) Von misses stress along the arms (e) percentage strain distribution along the arms

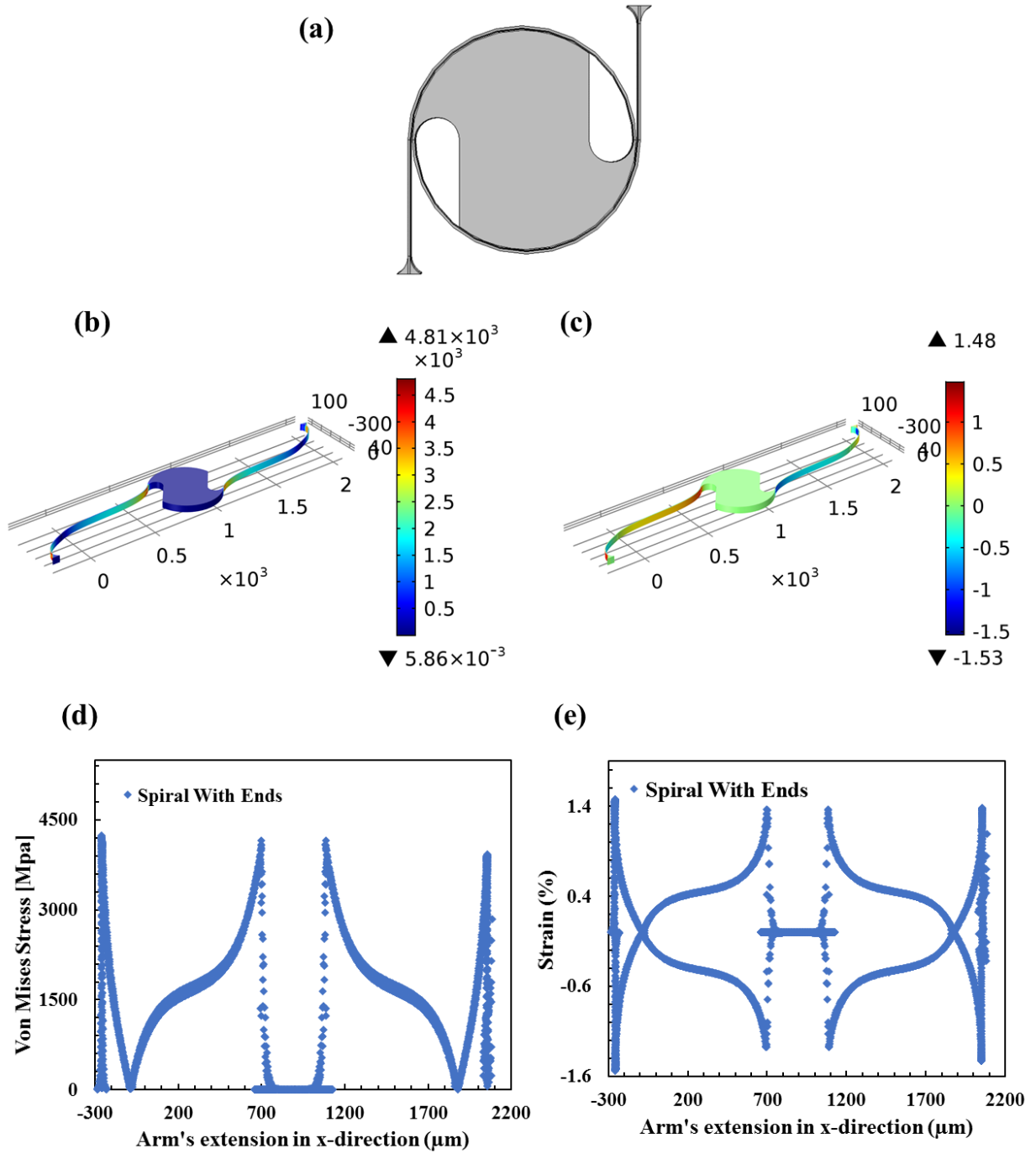


Figure 17 Spiral Structures with triangular-like ends (a) spiral structure with two arms (b) stress distribution along the arms (c) strain distribution along the arms (d) Von misses stress along the arms (e) percentage strain distribution along the arms.

At this point we were able to mark the area with highest stress and strain localization i.e. the end and the start of the arms. It is very crucial to have the minimum stress/strain at these points since, these are areas connected to the islands and also with the inner big circle of the spiral. Fig. 18 shows the comparison of spiral structures with and without the triangular-like ends. Fig. 18(a) shows the spiral structure with extended arms. Whereas, in Fig. 18(b) and Fig. 18(c) the comparison of stress and percentage strain is shown for the spiral with and without triangular-like structure at the end of the arms. This shows a clear reduction in the maximum peak stress and percentage strain. Therefore, our next step was to minimize that stress/strain localization at those crucial points and to design a more stretchable structure with even stress distribution along the arms.

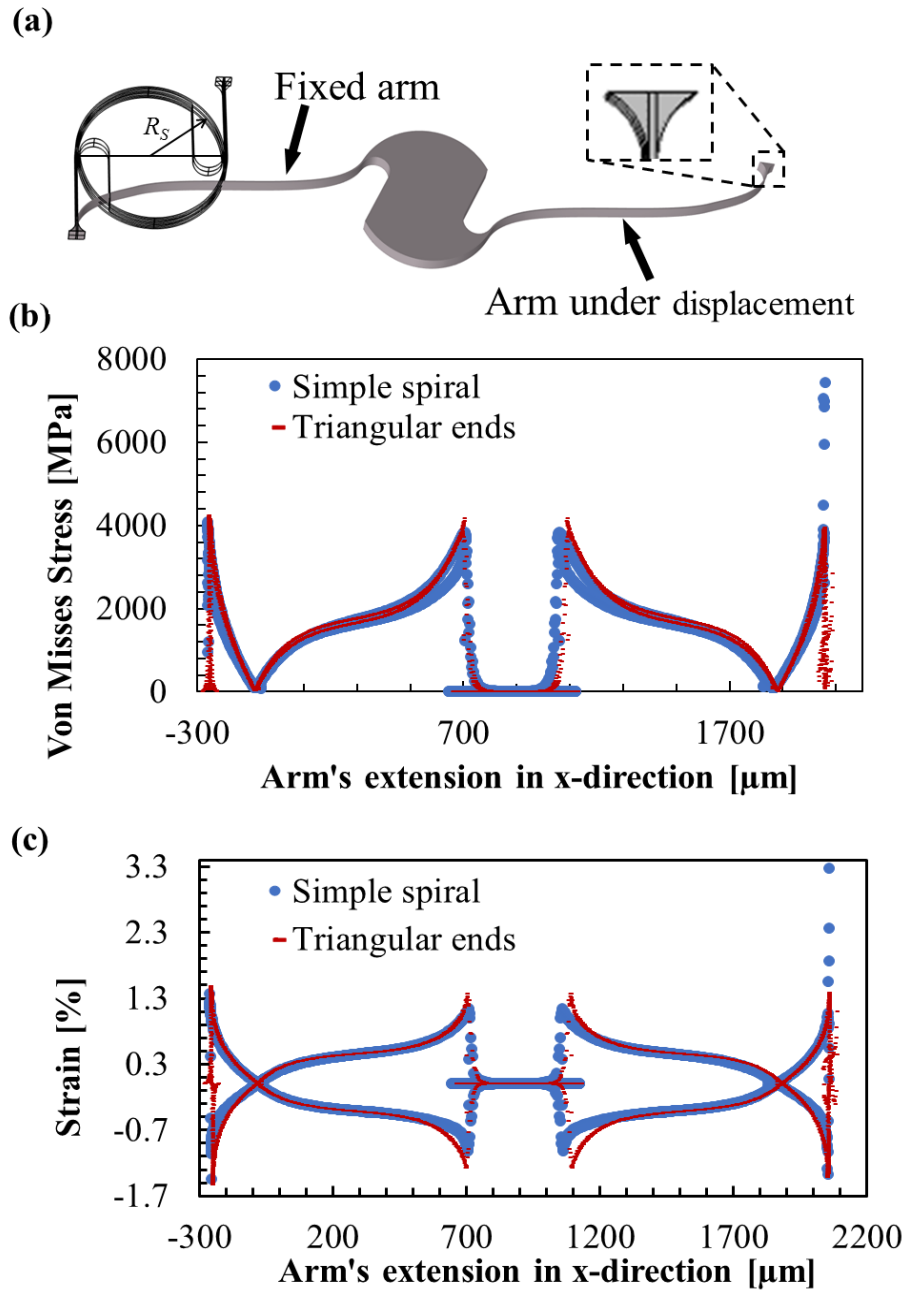


Figure 18 Comparison of Spiral structures (a) spiral structure with triangular ends with extended arms (b) comparison of stress distribution among two versions of spiral structure (c) comparison of stress distribution among two versions of spiral structure

### 3.2.2 Spiral with Unequal Halved Serpentine Arms

The next step after analyzing the spiral structure and noting its maximum stress localization points, was to replace the spiral's arms with different variants of serpentine structures. The version shown in Fig. 19(a) is a serpentine structure with each circular half having different radius represented by R1 and R2, with the values of 14.5 $\mu\text{m}$  and 9.5 $\mu\text{m}$  respectively. In this case, the trough is bigger (represented by R1) in size as compared to the crest (represented by R2). The structure, shown in Fig. 17(a), contains the serpentine structure where we replaced the straight arms of the spiral with serpentine ( $\alpha = L = 0$ ). The structure was simulated for its mechanical performance. Simulation results showed that this replacement resulted in great reduction in the maximum stress and strain localization. The Fig. 19(b) and Fig. 19(c) show the stress and stress distribution along the arms of the spiral-serpentine structure. The maximum value of the stress was found to be 2611.22 MPa, at the start of the serpentine arm that was subjected to the prescribed displacement, shown in Fig. 19(d). Similarly, the maximum value for percentage strain was found to be 1.03% at the start of serpentine arm under displacement, shown in Fig. 19(e). The simulations confirmed that the serpentine arms result in lower stress and strain localization and also uniform stress/strain distribution along the arms. Although, the stress and strain maximum value decreased, the maximum is still localized at the start of the arm.

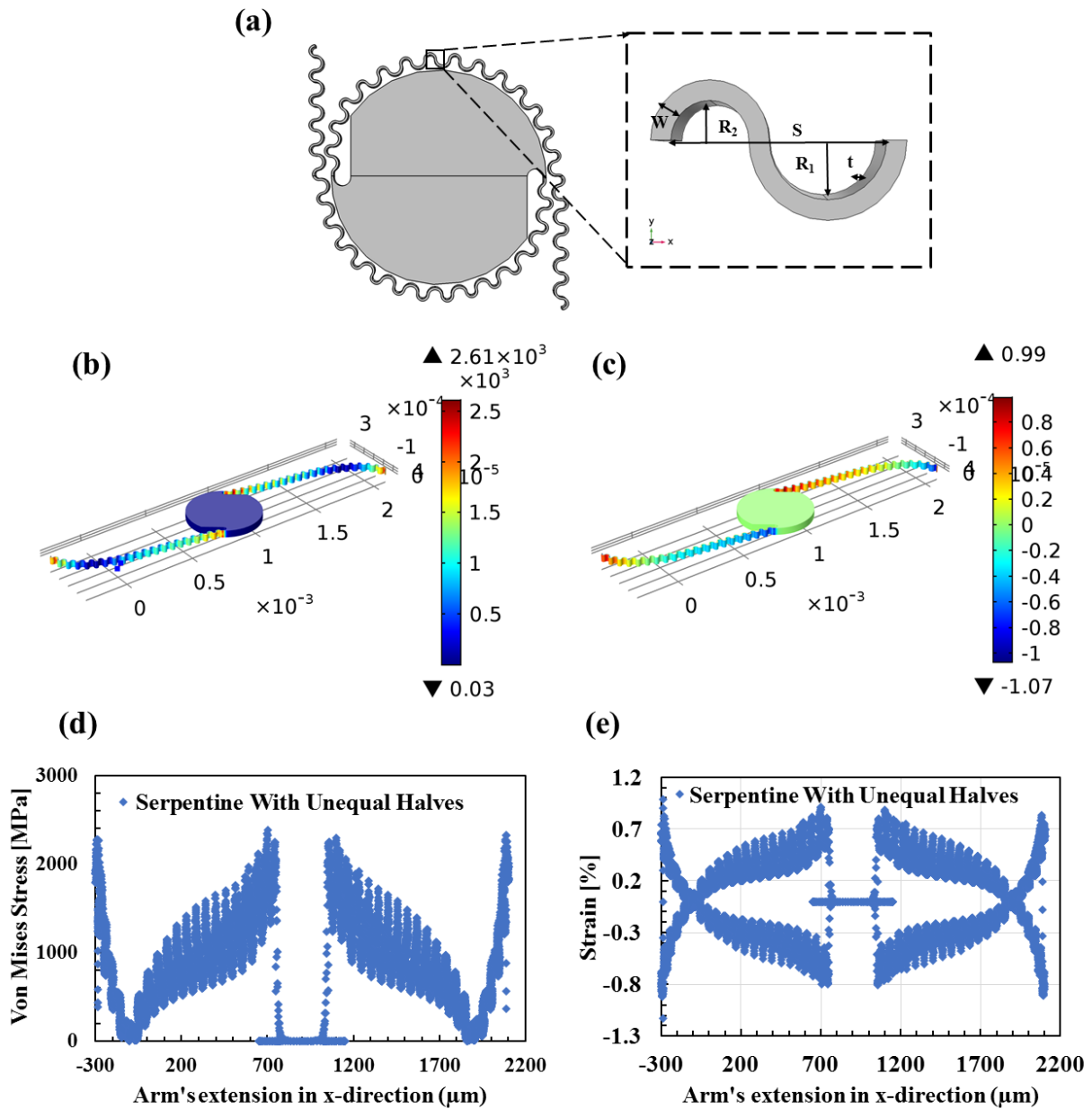
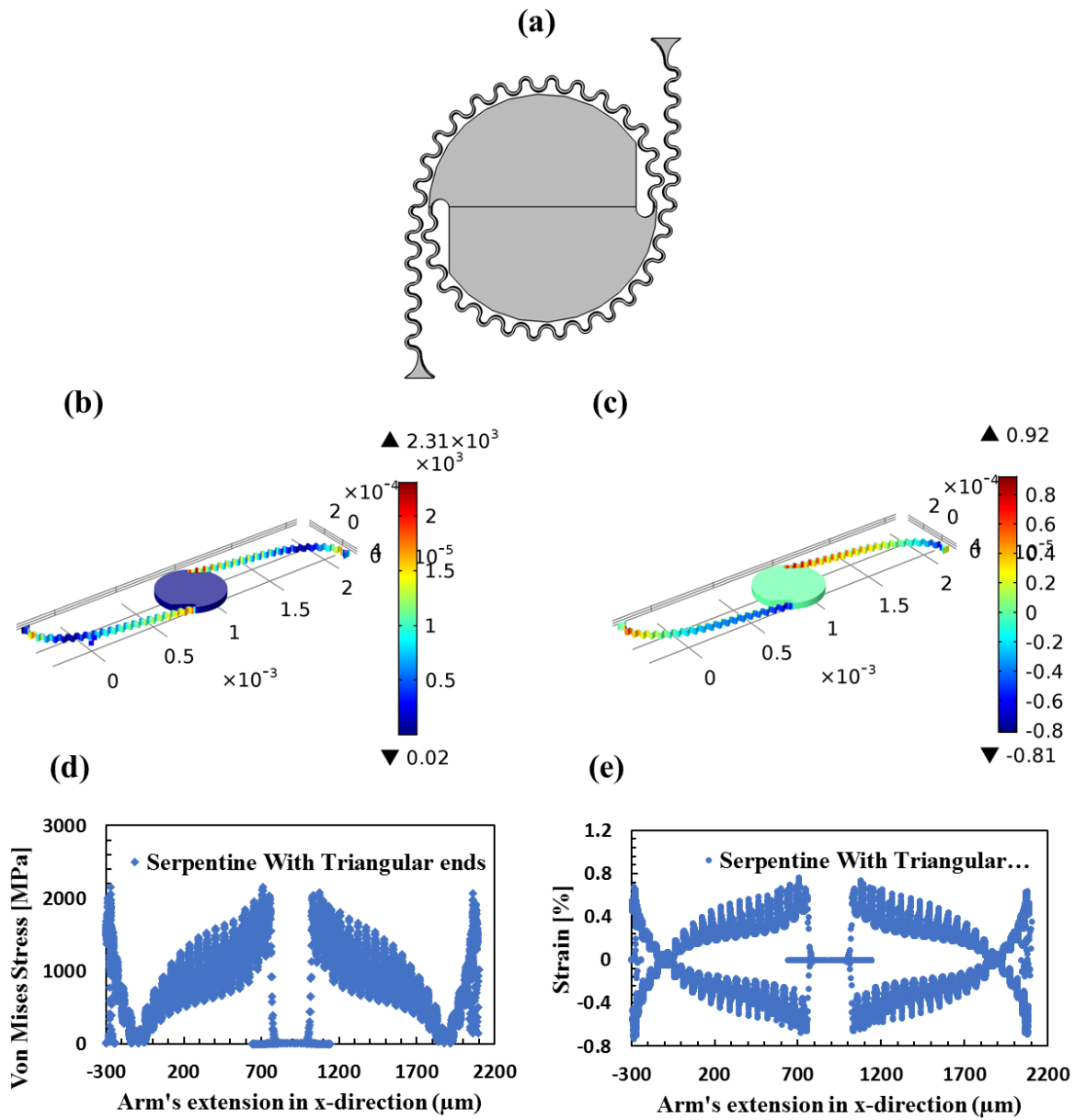


Figure 19 Spiral structures with serpentine arms with trough's radius bigger than crest (a) spiral structure with serpentine arms having unequal halves (b) stress distribution along the arms, (c) strain distribution along the arms (d) Von-Mises stress along the arms, (e) percentage distribution along the arms





**Figure 20** Spiral Structures with serpentine arms and triangular-like ends (a) spiral structure with two serpentine arms having unequal halves and with triangular-like ends, (b) stress distribution along the arms (c) strain distribution along the arms (d) Von-Mises stress along the arms, (e) percentage strain distribution along the arms

Since the ends of the arms will be connected to islands and the area of the structure (island) will be much higher as compared to the arm's width therefore, for smooth transition from lower to

higher width structure, we added a triangular like structure, like in Fig. 18(a). The resultant structure is shown in Fig. 20(a). The simulation resulted in lowering the maximum values of the stress and strain. Fig. 20(b) and Fig. 20(c) show the stress and strain distribution along the arms of the serpentine-spiral structure. The maximum stress in case of this unequal serpentine halves structure was found to be at the start of the spiral's arm under displacement with a value of 2309 MPa which is 46% less than the original spiral, shown in Fig. 20(d), while the maximum peak strain was found to be 0.93% at the start of the spiral's arm under displacement, which is 37.6% less than the original spiral, shown in Fig. 20(e).

It was observed that the maximum localization of the stress and strain was found to be at the areas where there is a transition from higher width ( $w$ ) to lower or vice versa. Therefore, in order to reduce the stress localization several modifications to the structure were made. In the structure shown in Fig. 21(a), we started the arm with a thickness of  $8\mu\text{m}$  and the decreased it to  $5\mu\text{m}$  gradually. The sole purpose of this modification was to shift the maximum stress localization away from the start of the arm. Although, the maximum stress value increased but it shifted the that point to the start of the triangular end, end of the arm that was kept fixed. The stress and strain distribution along the arms of the structure is shown in the Fig. 21(b) and Fig. 21(c) respectively. The maximum value of stress and strain were found to 2874 MPa and 1.08% at the to the start of the triangular end, at the end of the arm that was kept fixed, shown in Fig. 21(d) and Fig. 21(e). Similar modification, shown in Fig. 22(a), was made only at the end of the arms of the structure. Simulation results showed the shift in the maximum stress/strain to the start of the arm. Stress and strain distribution along the arm is shown in Fig. 22(b) and Fig. 22(c) respectively. The maximum values of the stress and strain were noted to be 2712.9 MPa and 1.07% at the start of the arm under displacement, shown in Fig. 22(d) and Fig. 22(e). Further, we combined modifications from the

Fig. 21(a) and Fig. 22(a). The maximum value of the stress and strain were found to be 3208 MPa at the 1.3%, respectively.

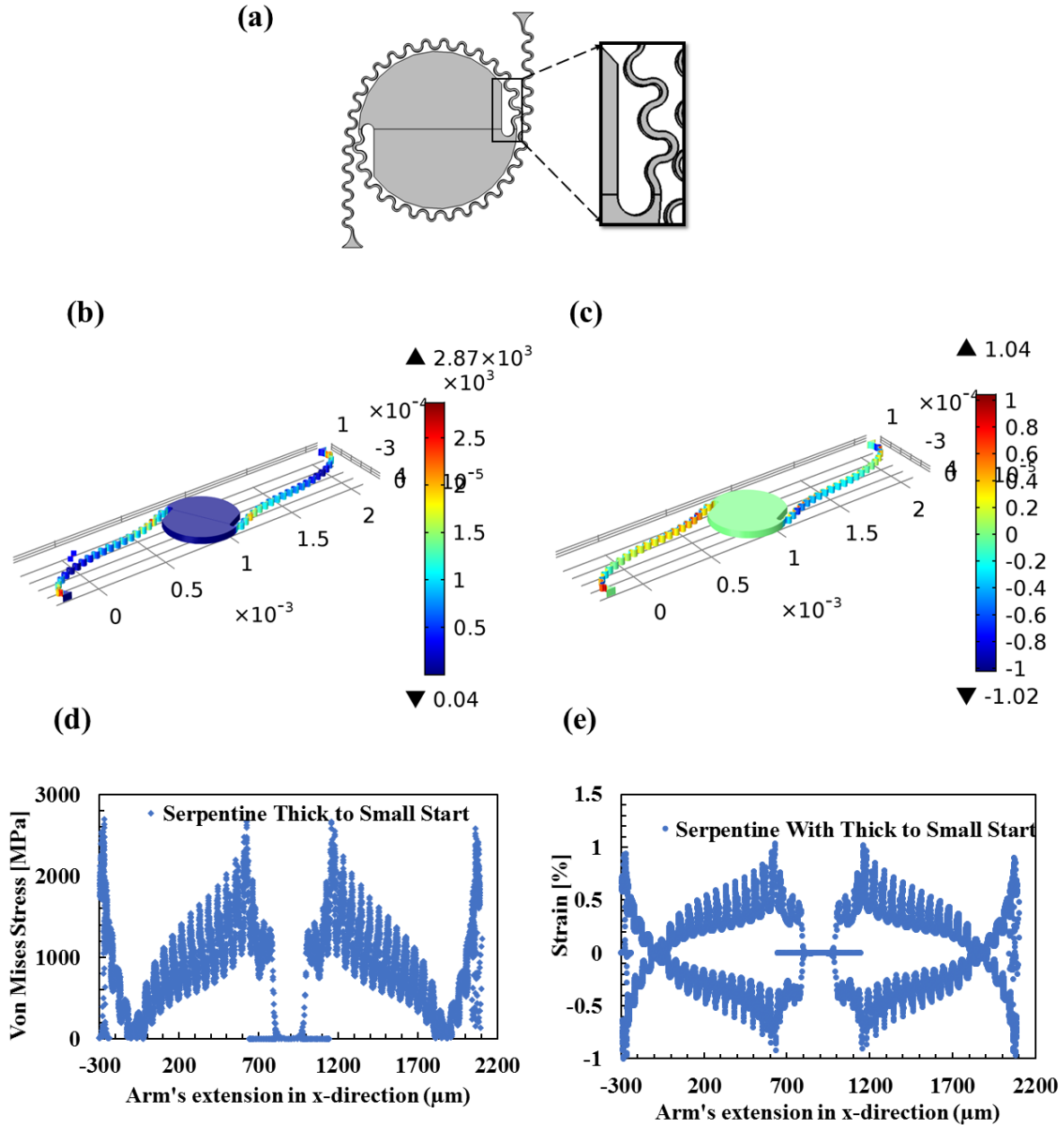


Figure 21 Spiral-serpentine compound structure with arm's thickness gradually decreasing at the start (a) spiral-serpentine compound structure with modified arm's start, (b) stress distribution along the arms (c) strain distribution along the arms, (d) Von-Mises stress along the arms, (e) percentage strain distribution along the arms.

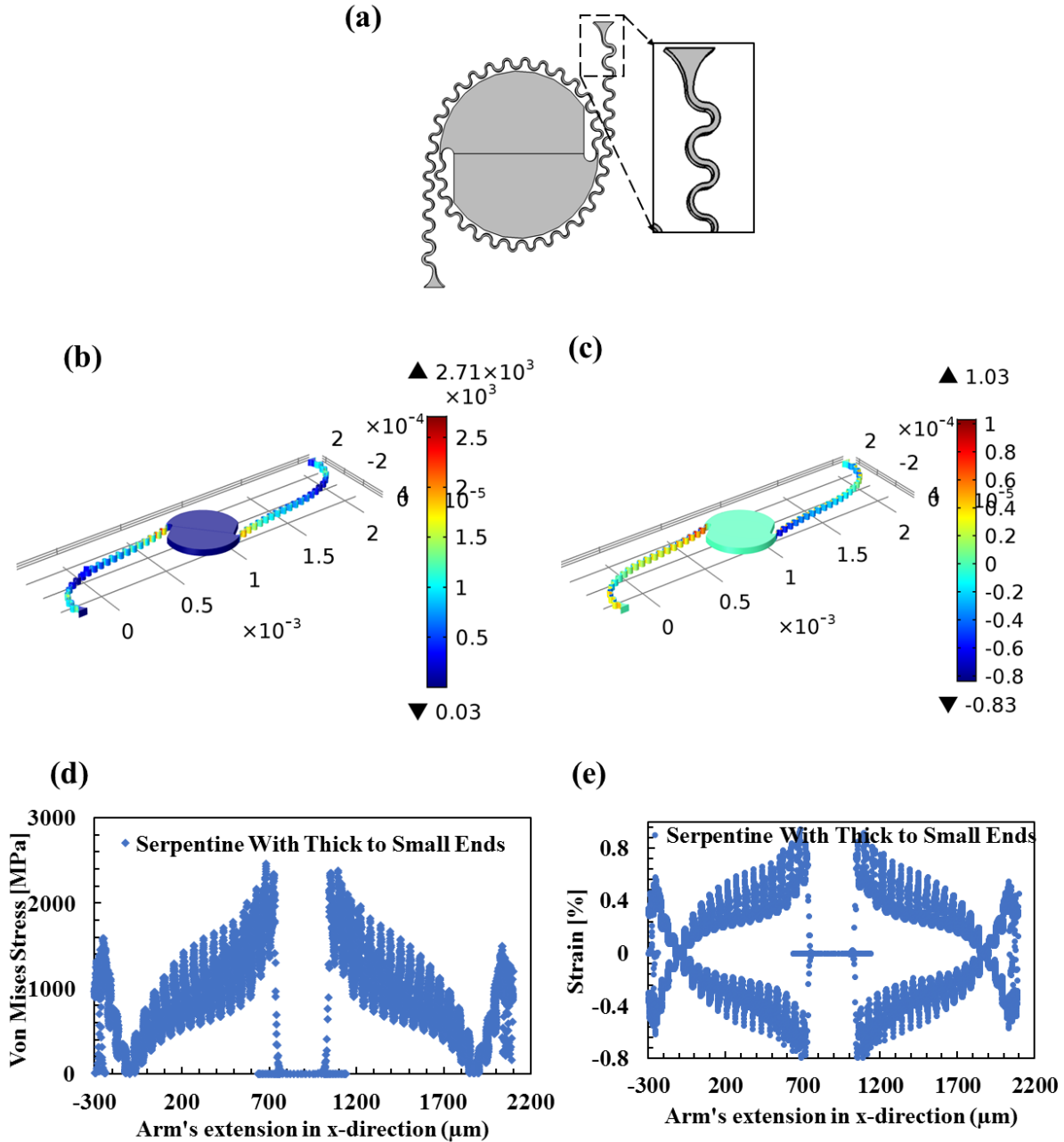


Figure 22 Spiral-serpentine compound structure with arm's thickness gradually increasing at the ends (a) spiral-serpentine compound structure with modified arm's end (b) stress distribution along the arms (c) strain distribution along the arms (d) Von-Mises stress along the arms (e) percentage strain distribution along the arms.

We also simulated the inverted structure version of the structure shown in the Fig.20(a) where crest is bigger in radius than the trough. The values of crest and trough are  $14.5\mu\text{m}$  and  $9.5\mu\text{m}$  respectively, shown in Fig.23(a). The highest value of the stress was 2382 MPa and the highest strain was 0.95%, both found at the start of the triangular end in the fixed arm, which are very

similar values to those where the crest is smaller than the trough (2309 MPa and 0.93%). Simulation results are shown in the Fig. 23(b), 23(c), 23(d), 23(e). We considered the structure shown in Fig. 20(a) for further optimization.

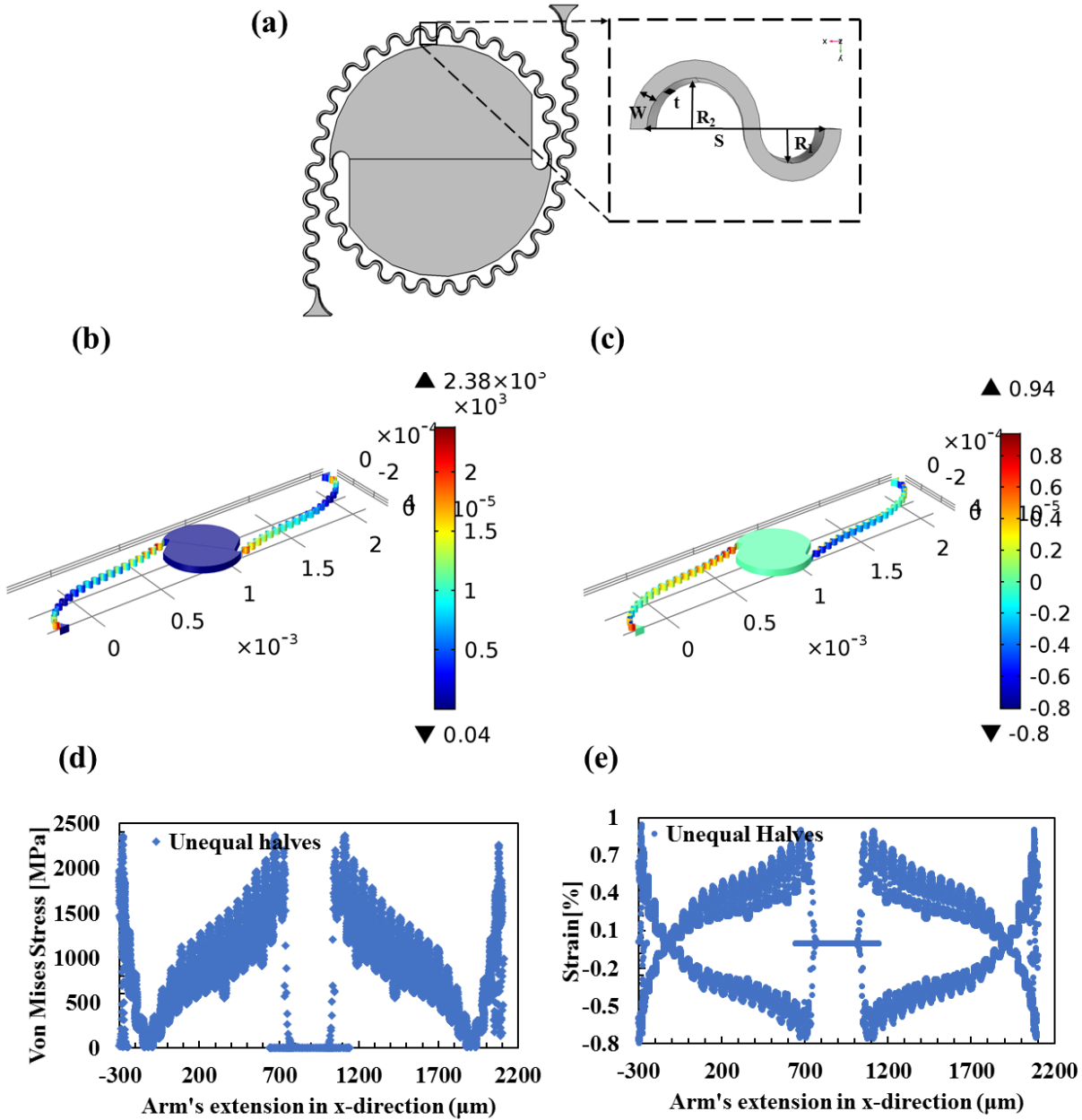


Figure 23 Spiral structures with serpentine arms with trough's radius smaller than crest (a) spiral structure with serpentine arms having unequal halves (b) stress distribution along the arms (c) strain distribution along the arms (d) Von-Mises stress along the arms (e) percentage strain distribution along the arms.

### 3.2.3 Spiral with Equal Halved Serpentine Arms

Another possible structure that we studied was with equal halves of the serpentine. In this case both the halves have the radius  $R=14.5\mu\text{m}$ , the longest radius, as shown in Fig. 24a). On the other hand, the structure with equal radius halves showed a reduced peak stress and strain, at the start of the spiral's arm under displacement, of 2265 MPa and 0.87% respectively, which represents a much higher respective reduction of 47.12% and 41% less than the original spiral structure. Simulation results are shown in the Fig. 24(b), 24(c), 24(d), 24(e). The comparison of the structure having serpentine with unequal halves from Fig. 21(a), and the one with equal halves from Fig 24(a) is shown in the Fig. 25(a). The comparison reveals that the serpentine with equal halves (with both half circles of equal radius) performs better than the one with unequal halves of the serpentine's half circles. The stress and percentage strain comparison on shown in Fig. 25(b) and Fig. 25(c), respectively.

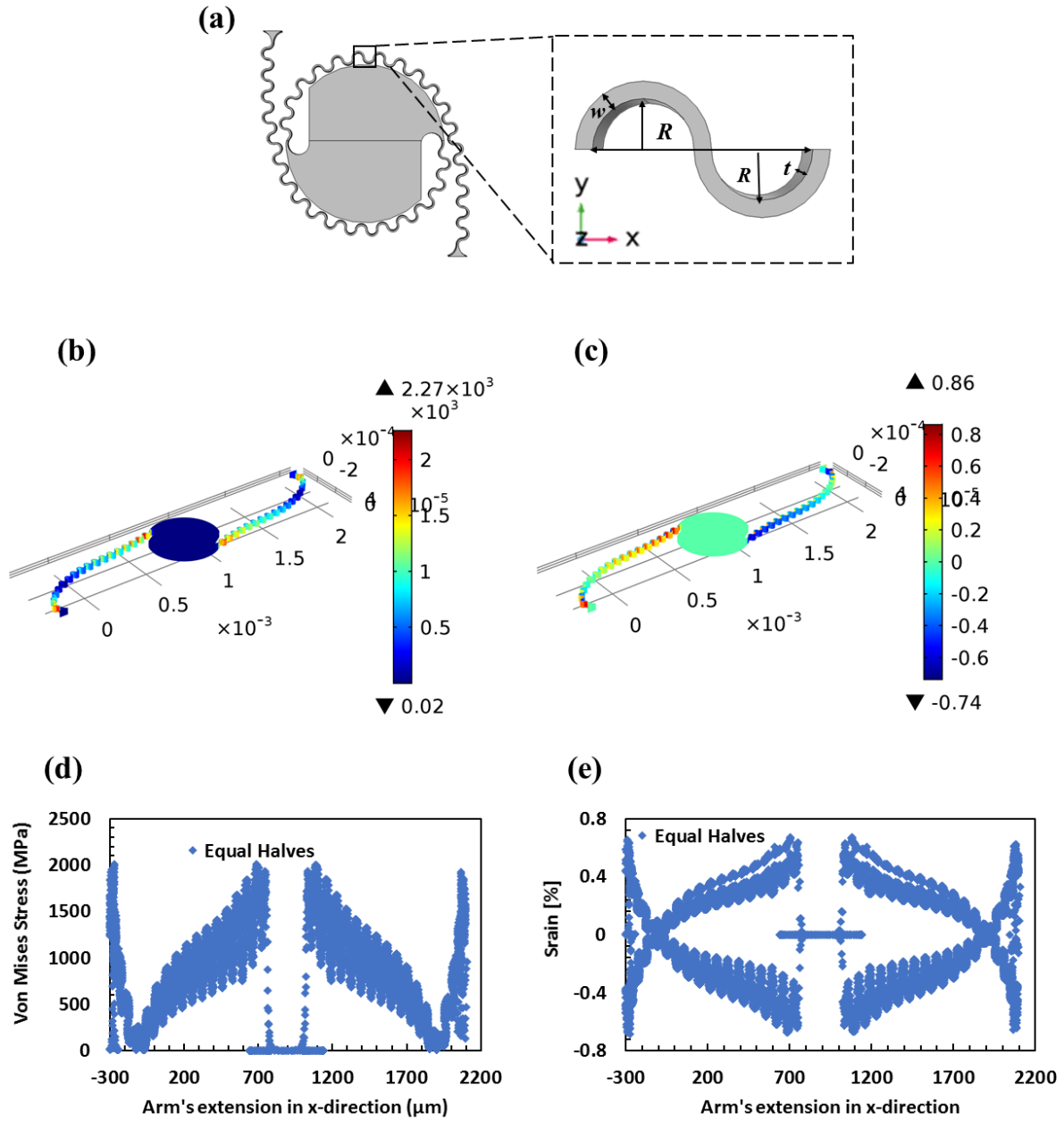


Figure 24 Spiral structures with serpentine arms having trough's radius equal to crest's radius (a) spiral structure with serpentine arms having equal halves (b) stress distribution along the arms (c) strain distribution along the arms (d) Von-Mises stress along the arms, (e) percentage strain along the arms.

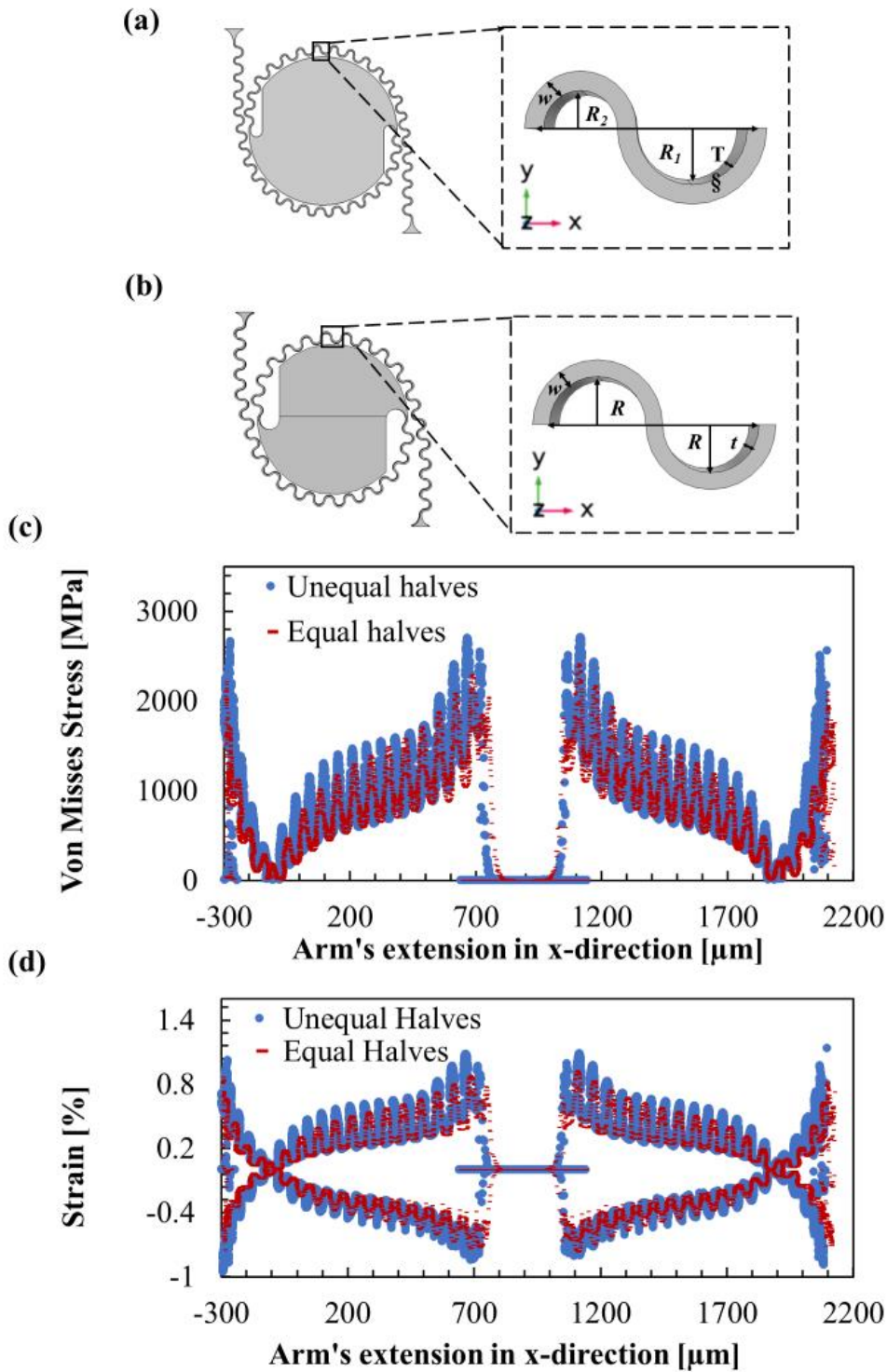


Figure 25 Comparison of Spiral-serpentine compound structure with equal and unequal halves (a) spiral-serpentine compound structure with serpentine arms having unequal halves (b) spiral-serpentine compound structure with serpentine arms having equal halves (c) comparison of Von Mises stress along the arms (d) comparison of percentage strain distribution along the arms.



As mentioned above, the radius of the arch of the serpentine plays a very important role in the performance of the structure (see eq. 3.2 and eq. 3.3). Therefore, another possible modification, to improve the stress/strain localization and to distribute the stress evenly throughout the arms, is to add a bigger structure, with larger radius, at the points with larger stress/strain. Horseshoe, a structure with a bigger radius, is a better choice considering the geometry of the serpentine. Therefore, we optimized the structure, shown in Fig.24(a), in order to reduce the stress localization. The resultant structure is shown in Fig. 26. In Fig. 26(a), the end points were replaced with the horseshoe structure and simulation results show that the reduction in maximum stress and strain. As shown in Fig 26(c), the point of maximum stress was shifted to start of the serpentine's arm. The maximum stress and strain was found to be 2328 MPa, and 0.9%, respectively. Another modification to the structure in Fig.24, was to add a horse shoe at the start of the serpentine's arm along with changing the starting point. The resultant structure, shown in Fig. 26(b), also showed a decrease in stress and strain values. The maximum stress and strain values were observed to be 1996 MPa, and 0.74%, respectively. Finally, a structure containing equal halves of the serpentine and horseshoe structure both at the start and beginning of the arm was analyzed for its stress and strain distribution. The resultant structure and simulation results are shown in the Fig. 27. Fig. 27(b), Fig. 27(c), Fig. 27(d), Fig. 27(e) represent the simulation results. The maximum values for the stress and strain due to the incorporated modifications were observed to be 1821 MPa and 0.70%. Based on the simulation it could be inferred that serpentine structure provide better results in terms of stress and strain distributions as compared to the simple spiral structure. Moreover, by replacing serpentine with more horseshoe structure at the beginning and end could result into the maximum stress localization away from the beginning as well end of the arm.

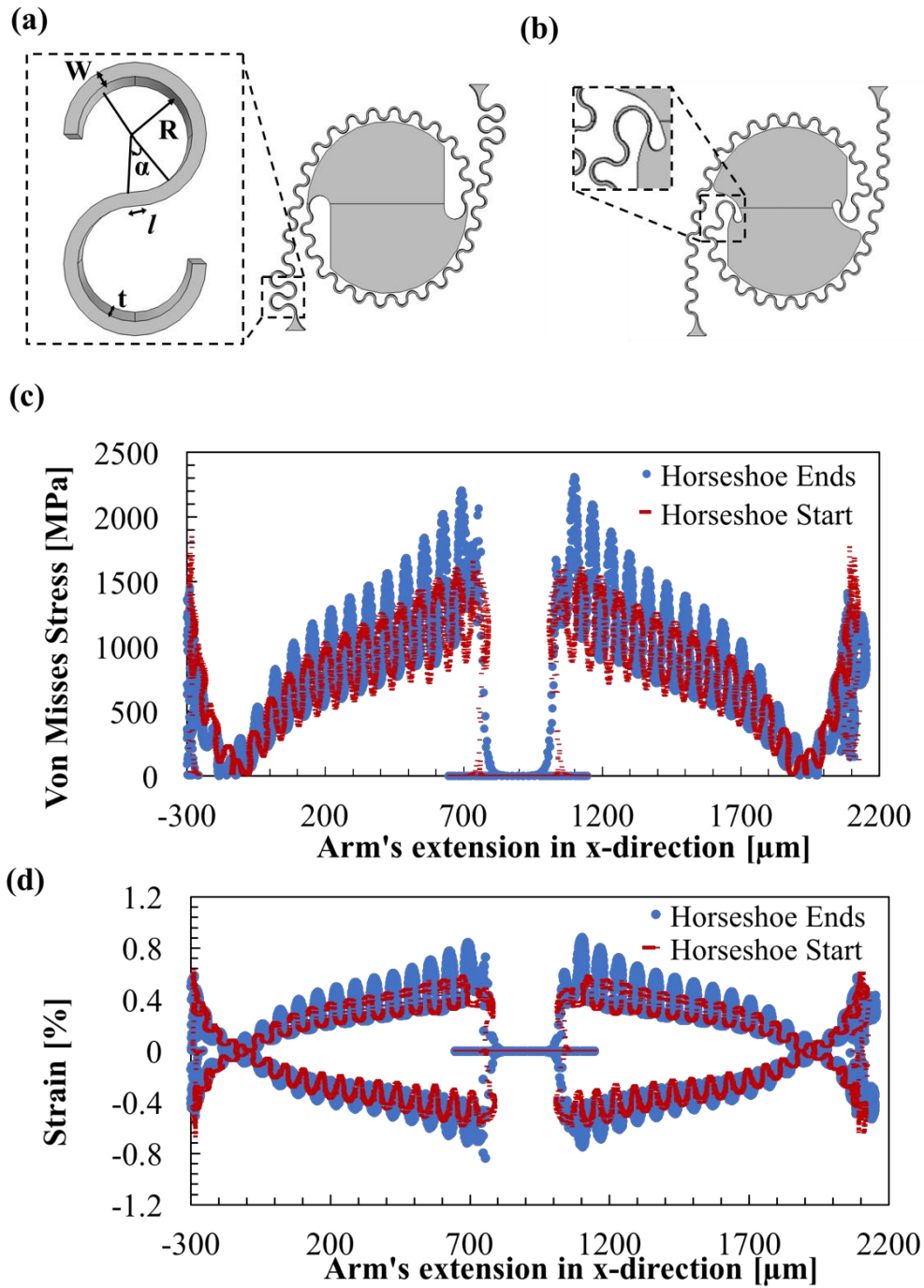


Figure 26 Spiral-serpentine compound structure with equal serpentine halves and horseshoes at the end/beginning of arms. Schematics of (a) serpentine/spiral structure with horseshoe at the end, and (b) with horseshoe at the start. (c) Stress comparison along the arms, (d) strain distribution comparison along the arms.

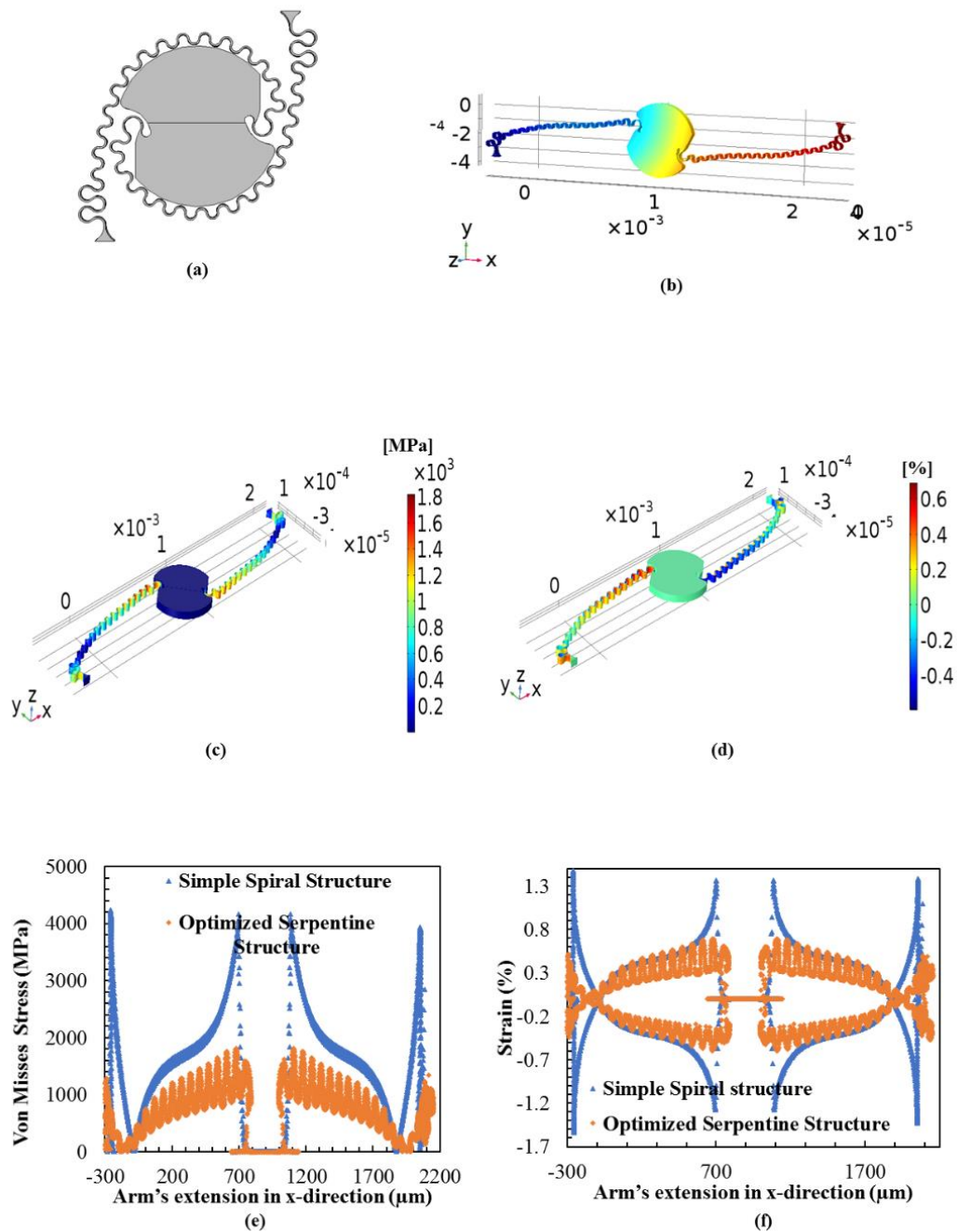


Figure 27 Spiral-serpentine compound structure with equal serpentine halves and horseshoes at the beginning and end of the arms. Schematics of (a) serpentine/spiral structure with two arms and horseshoe structure, and (b) stretched structure. (c) 3D stress distribution along the arms, and (d) 3D strain distribution along the arms. (e) Stress comparison between original spiral and compound structure along their arms, and (f) strain distribution comparison between original spiral and compound structure along their arms.

Finally, Fig.28 shows the comparison and summary of all the designs where the simple spiral shows the maximum stress/strain but with the addition of the triangular-like end, both stress and strain were reduced significantly. Moreover. Addition of serpentine to the simple spiral's arm reduced the stress and strain values further. It is also evident from Fig. 28 that starting with a thicker thickness and gradually decreasing it, either at the start or at the end, it didn't reduce the stress as much as compared to other designs. Finally, the designs with horseshoe resulted in the lowest values of stress as well as strain.

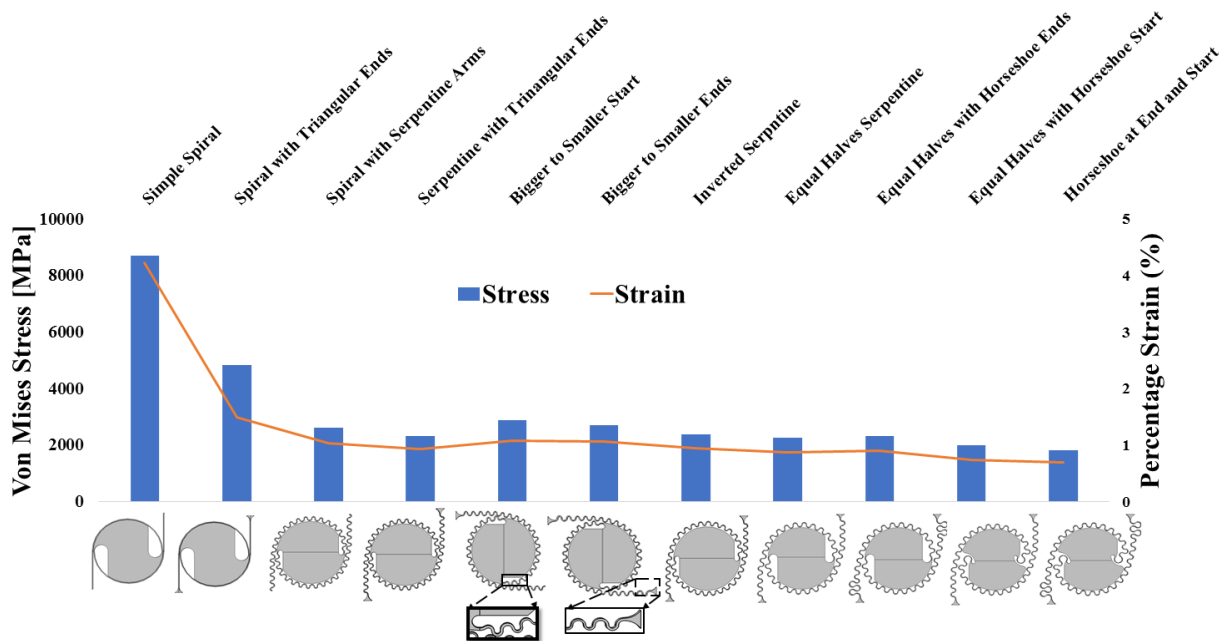


Figure 28 Summary of the spiral based designs

# CHAPTER

## FABRICATION

This chapter will explain the fabrication process for spiral based structure for stretchable electronics. Structures were fabricated using mono-crystalline silicon and SOI. The process begins by preparing the mask for the structure that is to be written on the wafers during the photolithographic process. Series of steps will be followed in order to release the structure from the wafers. The process will be validated through the SEM of the structures before and after the release.

### 4.1 Fabrication Process Description

#### 4.1.1 Mask Design

To fabricate a structure, we started with the preparation of the mask using Tanner EDA L-edit. The mask contains two sets of six structures. First set contains three structures each with hexagonal Islands while the rest of three contain square islands. In each structure the size of interconnecting spiral varies. The first structure contains the spiral with radius 250 $\mu\text{m}$  and arm's thickness of 5 $\mu\text{m}$  as shown in the Fig. 29. In the other structure, the size of each element was doubled for example the spiral's radius was 500 $\mu\text{m}$  and arm's thickness of was 10 $\mu\text{m}$ . While in the third variant we increased the number of turns to 2 as shown in the Fig. 30. All these three structures were repeated for square islands as shown in Fig. 31. Moreover, each structure was patterned with hole of radius 10 $\mu\text{m}$  in diameter. These holes will later facilitate the etching and releasing of the structures.

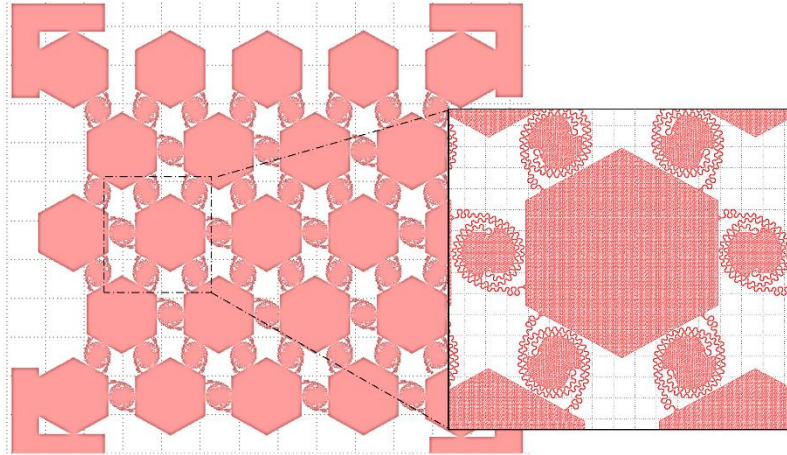


**Figure 29 Hexagon interconnected through single turn spirals**

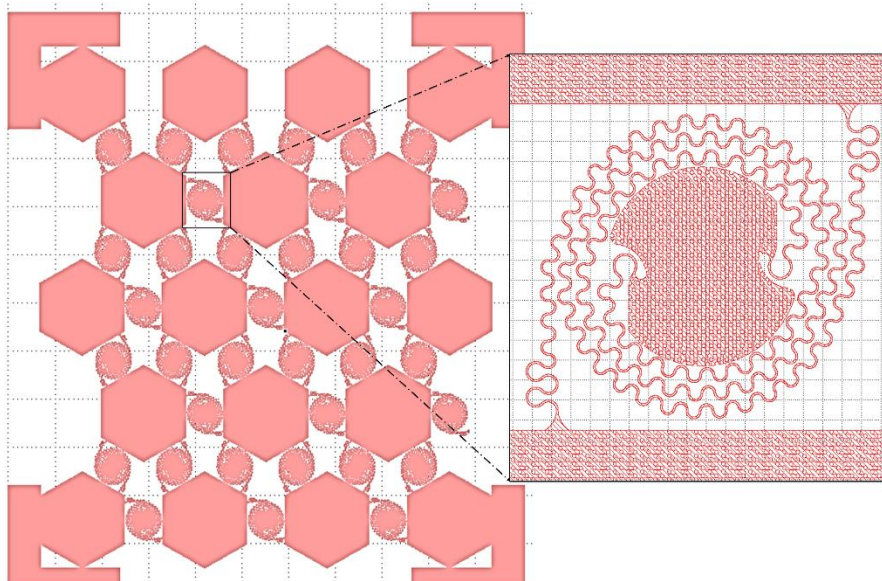


**Figure 30 Hexagon interconnected through multi-turn spirals**

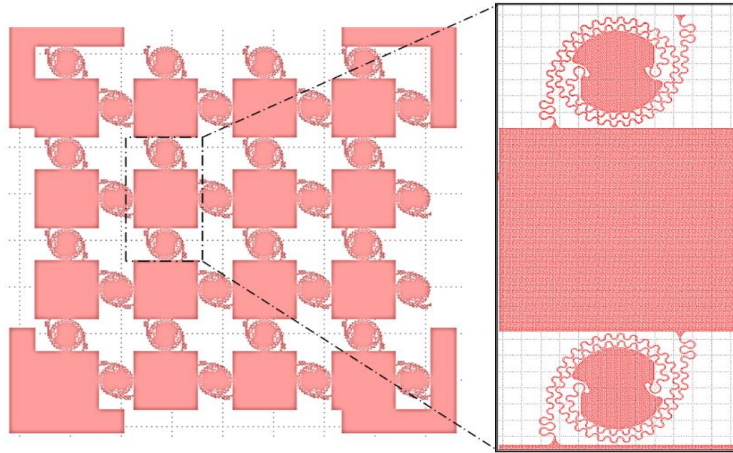
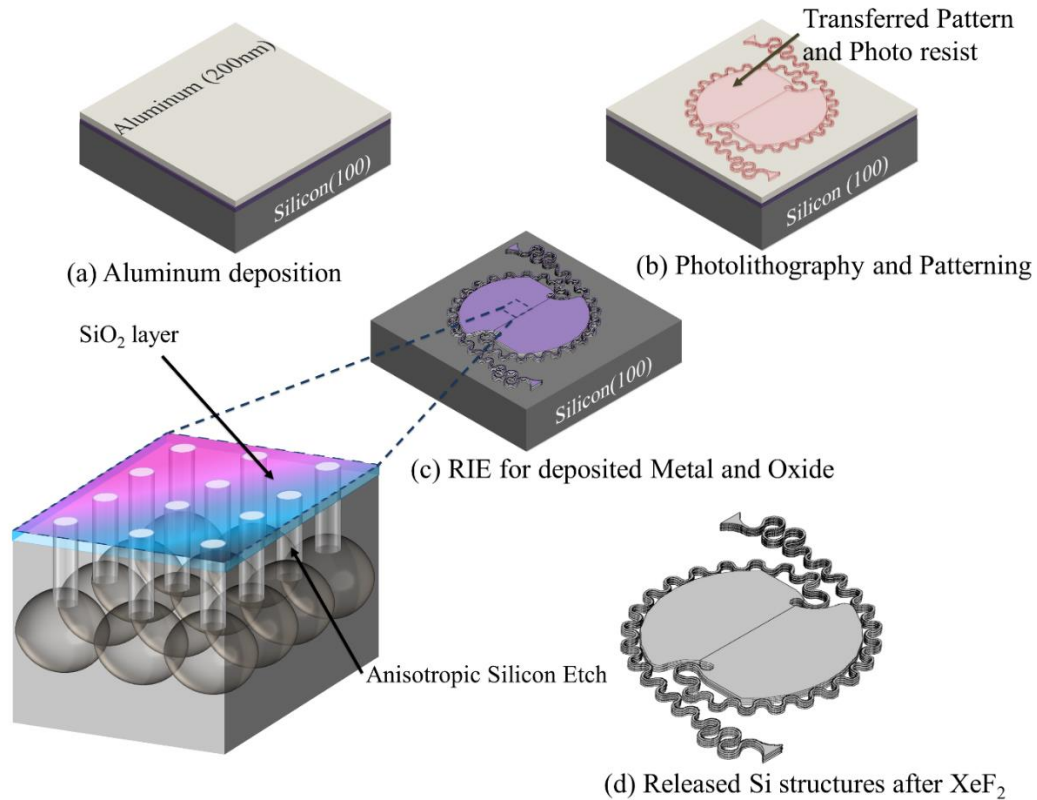


Figure 31 Hexagon interconnected through single turn.

#### 4.1.2 Fabrication Process For Si (100) Wafer

As mentioned earlier the fabrication was done on two wafers, mono-crystalline bulk silicon and SOI, with each one having a different fabrication flow. Mon-crystalline bulk silicon (100) is a cheaper wafer where the electronic devices are fabricated on the top surface of the wafer. It has excellent electrical and mechanical properties. Thin sheet, containing the electronic devices or structures, can be peel off from the surface of the bulk through a controlled fabrication process. On the other hand, SOI is an expensive option with excellent properties. It has a buried oxide layer and electronic devices are fabricated on the silicon thin layer on top of buried oxide. The oxide layer acts as an insulator and improves the electrical properties of the devices fabricated. Moreover, thin silicon layers, above the oxide layer, can easily be removed through controlled fabrication process.





**Figure 32 Fabrication flow for releasing Spiral-serpentine structure from mono-crystalline silicon wafer.**

We started the process with 4" mono crystalline silicon wafer. The fabrication flow for mono-crystalline silicon shown in Fig. 32. In order to protect the silicon, 500nm thick silicon dioxide (SiO<sub>2</sub>) was grown on 550μm thick silicon through the wet-dry-wet technique. This SiO<sub>2</sub> layer will act as hard mask later in the process and will protect the silicon layer especially during the release of the structure using Xenon difluoride (XeF<sub>2</sub>). Next, we deposited 200nm Aluminum (Al) on top of SiO<sub>2</sub> through physical deposition (400 W<sub>RF</sub>, 600 seconds, 5 mTorr, Pre-sputter: 100 seconds, 25 sccm Ar), shown in Fig. 32(a). This metal was deposited as hard mask for silicon layer to protect the silicon during the deep reactive ion etching (DRIE) process. In order to pattern the structure on the wafer, next step was the deposition of 4μm ECI3027 photoresist on the metal layer through spin coating at the spin speed of 1750 rpm for 30sec and soft baking for 60sec at 100°C. Next the pattern was transferred to the wafer using the photolithography, shown in Fig.32 (b). Once the



structure was deposited on the wafer, photoresist was washed with a solvent to remove the area that was not a part of the pattern. In order to prepare the wafer for DRIE, holes that were drawn during the mask making must not contain any metal or oxides. The purpose of these holes is to provide a path for the gases to diffuse into the structure to etch the material deposited beneath. The type of the gas used depends on the material to be removed. Therefore, to clean the holes, reactive ion etching (RIE) process was used to first etch the top Al through chlorine ( $\text{Cl}_2$ ) containing gases (100  $\text{W}_{\text{RF}}$ , 40 mTorr, 10 sccm  $\text{Cl}_2$ , 40 sccm  $\text{BCl}_3$  and 5 sccm Ar).  $\text{BCl}_3$  provides a protective layer by depositing a polymer to protect the silicon during the etch while  $\text{Cl}_2$  etched the Al layer deposited in the first step. Whereas, the inert gas Ar was used to provide the plasma required for etching. Similarly, the oxide layer deposited at the start must be removed to clear the holes using oxide RIE (100  $\text{W}_{\text{RF}}$ , 30 mTorr, 40 sccm  $\text{C}_4\text{F}_8$ , 5 sccm  $\text{O}_2$ ). For DRIE, gases containing the fluorine were used to etch the silicon anisotropically (5 sccm  $\text{C}_4\text{F}_8$ , 100 sccm  $\text{SF}_6$ , 30 mTorr, 30  $\text{W}_{\text{RF}}$ ). The schematic is shown in Fig. 31(c). In the inset of Fig. 32(c), where the vertical channels represent the etched silicon anisotropically. Fig. 33 shows the SEM image of the vertical channels formed during the DRIE. Whereas Fig. 34 shows the SEM of spiral connected with square islands. The images shown in Fig. 35 and Fig. 36 show a closer view of the structure after the DRIE. It also shows the effectiveness of the process without any damage to the structure.

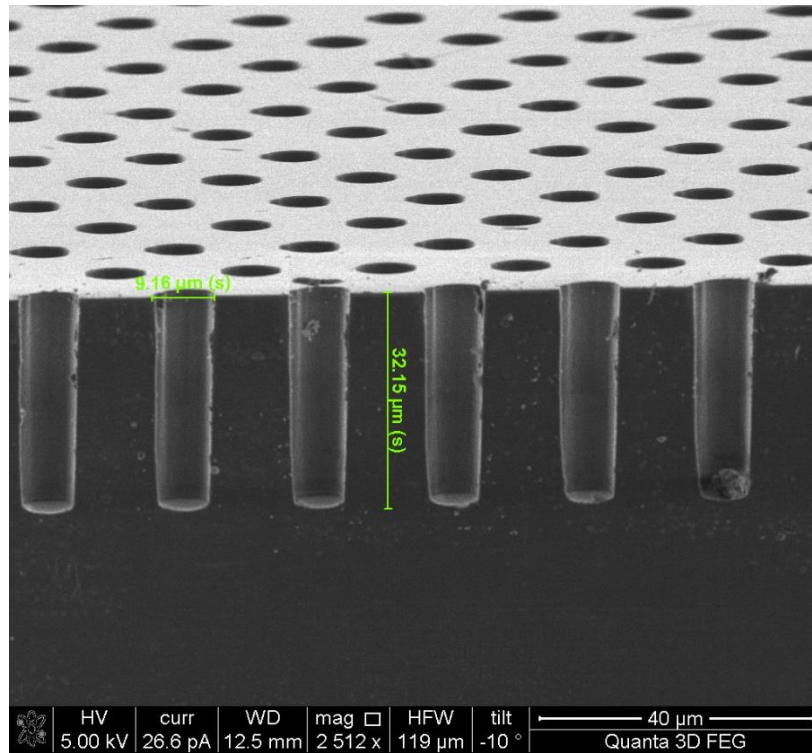


Figure 33 SEM of the DRIE for mono-crystalline Silicon.

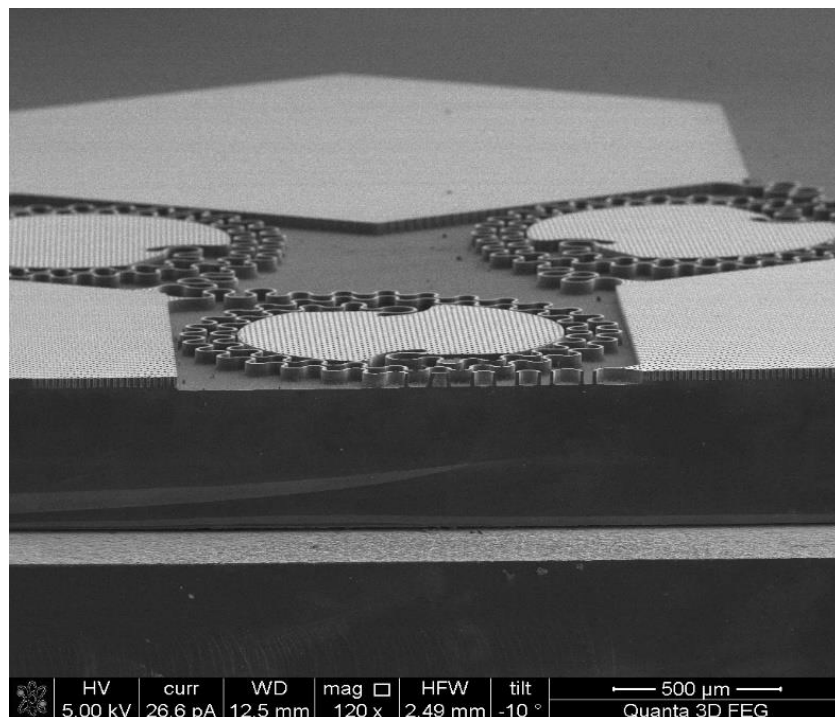


Figure 34 SEM of spiral interconnects after DRIE for mono-crystalline Silicon.

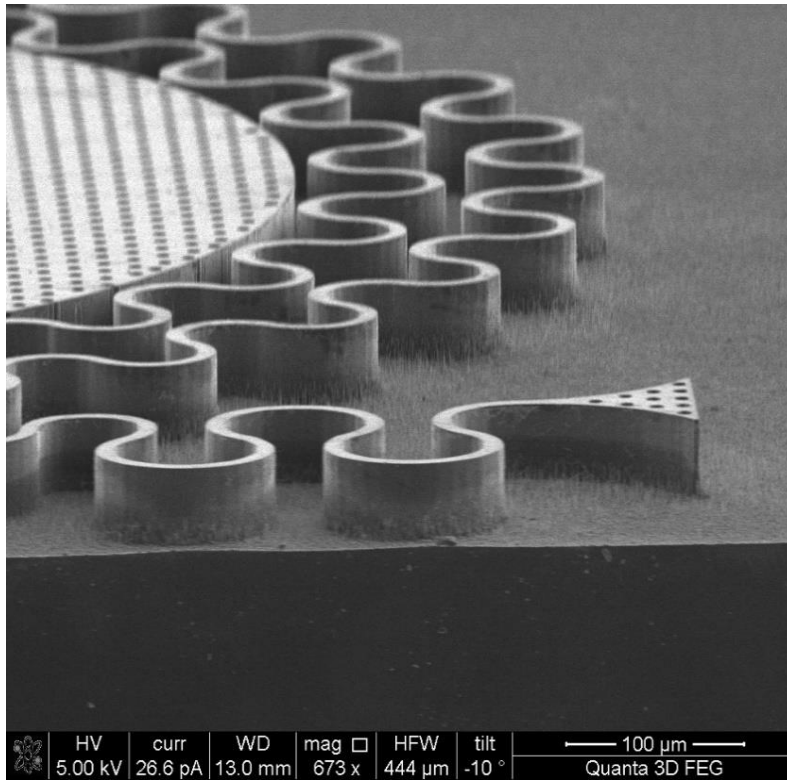


Figure 35 SEM of the spiral structure after DRIE for mono-crystalline silicon.

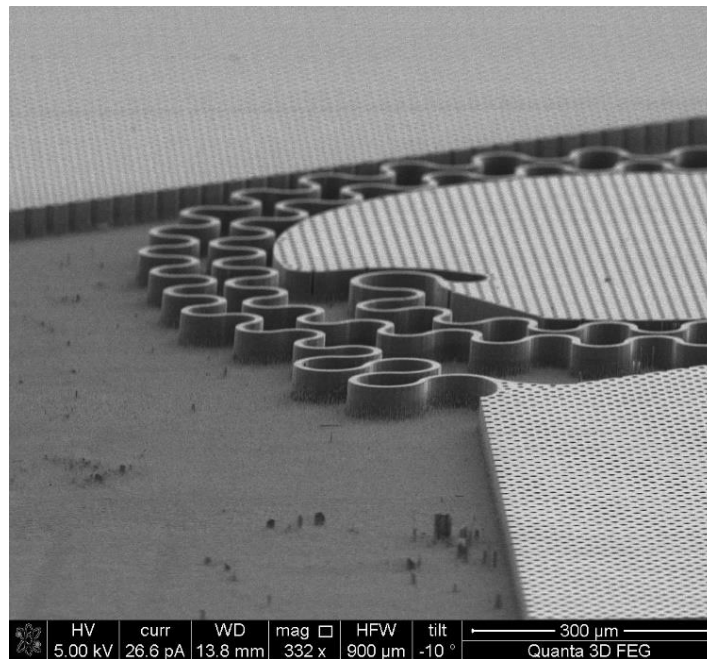
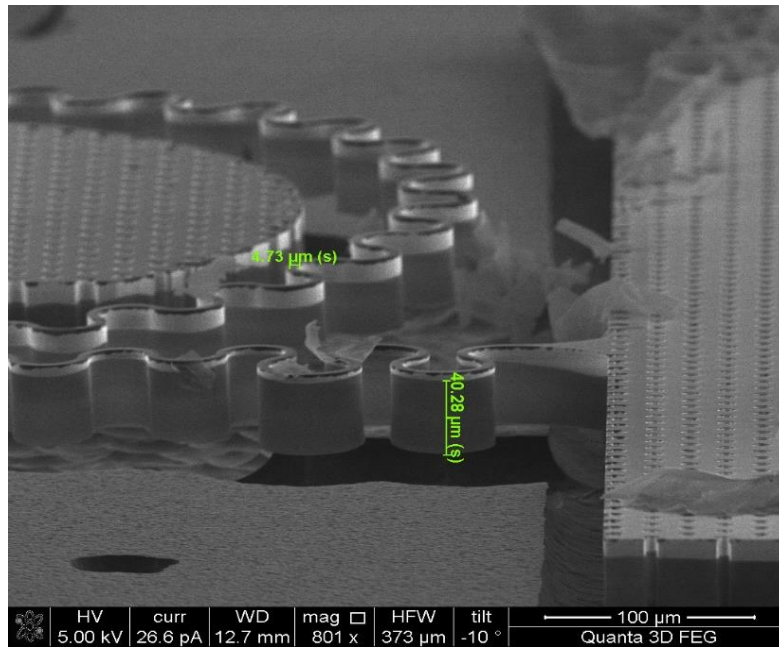


Figure 36 SEM of spiral with Island after DRIE for mono-crystalline Silicon.

Before starting releasing of the structure from the wafer, the sides walls of the tunnels must be protected to avoid any lateral loss of the silicon. Therefore, 45nm thick  $\text{Al}_2\text{O}_3$  was deposited using atomic layer deposition method and then by using the highly directional RIE to etch the  $\text{Al}_2\text{O}_3$  from the bottom (40nm/min, 4 m Torr, 20 sccm  $\text{CHF}_3$ , 5 sccm Ar). And finally, the structures were released using  $\text{XeF}_2$  isotropic etching (85 cycles, 30sec/cycle, 4m Torr). It etched the silicon below the channels laterally as well as vertically and the final structure was released from the silicon. The SEM images shown in Fig. 37, Fig. 38, Fig. 39, Fig. 40, and Fig. 41 show the etched structure from the mono-crystalline silicon wafer.



**Figure 37 SEM of spiral after release.**

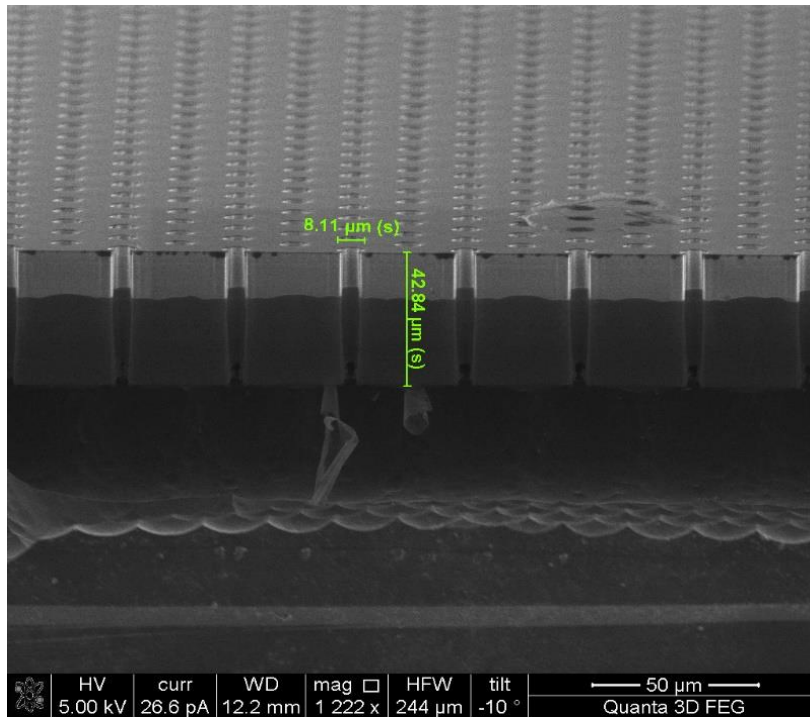


Figure 38 SEM of the Square Island after release

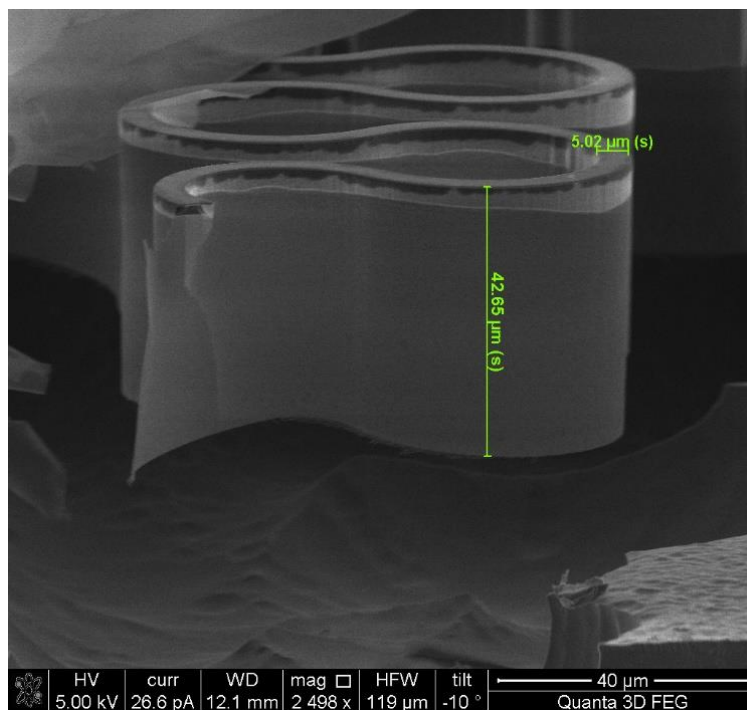
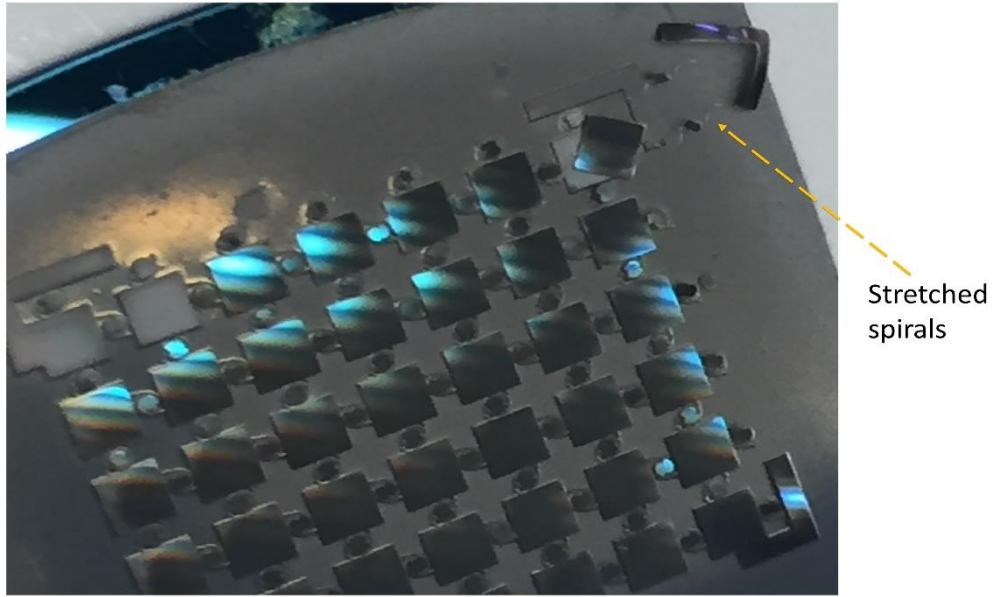
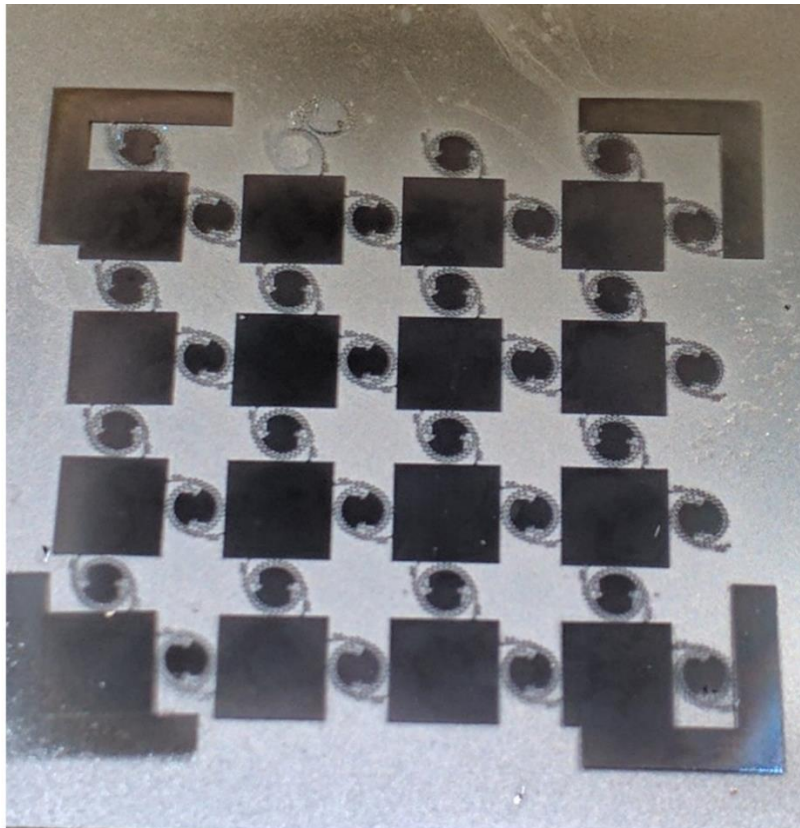


Figure 39 SEM of the spiral's horseshoe after release.





**Figure 40 Structure released from mono-crystalline Silicon.**



**Figure 41 Structure released from mono-crystalline Silicon.**

### 4.1.3 Fabrication Process For SOI Wafer

In the second approach, we used SOI wafer (50  $\mu\text{m}$  of Silicon on top of  $\text{SiO}_2$ ). The schematic flow of the process is shown in Fig. 42.

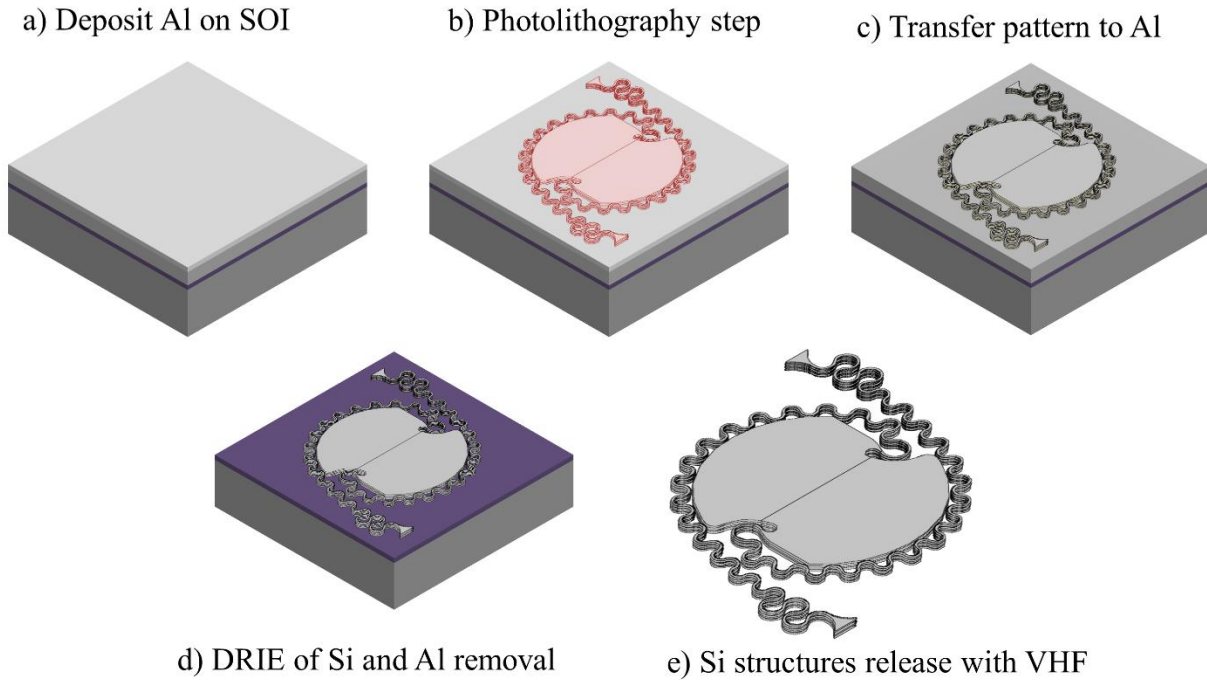


**Figure 42** Fabrication process flow for the silicon on insulator (SOI) wafer.

We started the process by the deposition of Al through sputtering (400  $W_{\text{RF}}$ , 600 seconds, 5m Torr, Pre-sputter: 100 seconds, 25 sccm Ar). Secondly, the 4 $\mu\text{m}$  thick photoresist ECI3207 was deposited using the spin coating at the spin speed of 1750 rpm for 30 seconds and soft baking for 60 seconds at 100°C. The structure was patterned and then the photoresist was removed by acetone and ashing (0.5 Torr, 100°C, 100 sccm  $\text{O}_2$ , 1 sccm  $\text{CF}_4$ , 14 sccm Ar). The next step was RIE for Al (50  $W_{\text{RF}}$ , 40 m Torr, 10 sccm Cl, 30 sccm  $\text{BCL}_3$ , 5 sccm Ar). In the next step, the anisotropic

etching of silicon was carried out (5 sccm  $C_4F_8$ , 100 sccm  $SF_6$ , 30 mTorr, 30  $W_{RF}$ ) shown in Fig. 43. Once the silicon was etched we removed the Al using RIE (100  $W_{RF}$ , 40m Torr, 10 sccm  $Cl_2$ , 40 sccm  $BCl_3$  and 5 sccm Ar). The last step was the release of the structure using vapor hydrofluoric acid (VHF) for 2 hours and the structure was released finally shown in Fig. 44. Finally, in order to validate the fabrication process, we stretched one of the square island structure interconnected with single turn compound spiral-serpentine structure as shown in Fig. 45. While keeping one island fixed and subjecting the other to move to a stretchability of almost 470%. This validated the effectiveness of proposed design as well as the fabrication process.

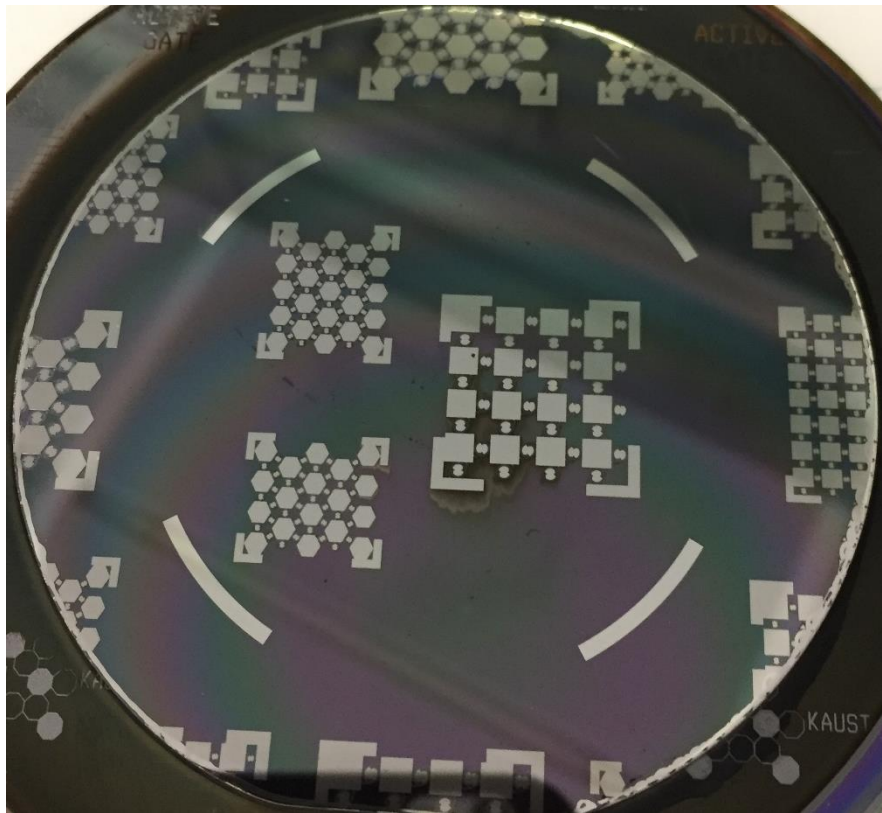


**Figure 43 SOI wafer after the DRIE of Silicon.**



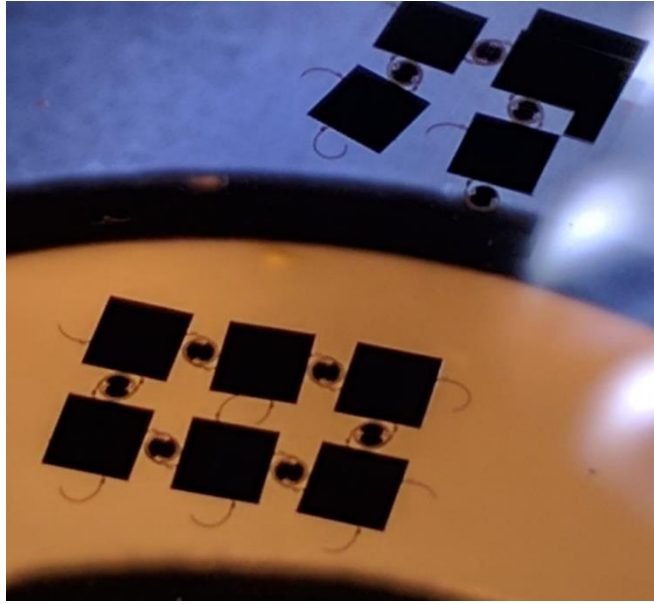


Figure 44 Released Square structure from SOI wafer.

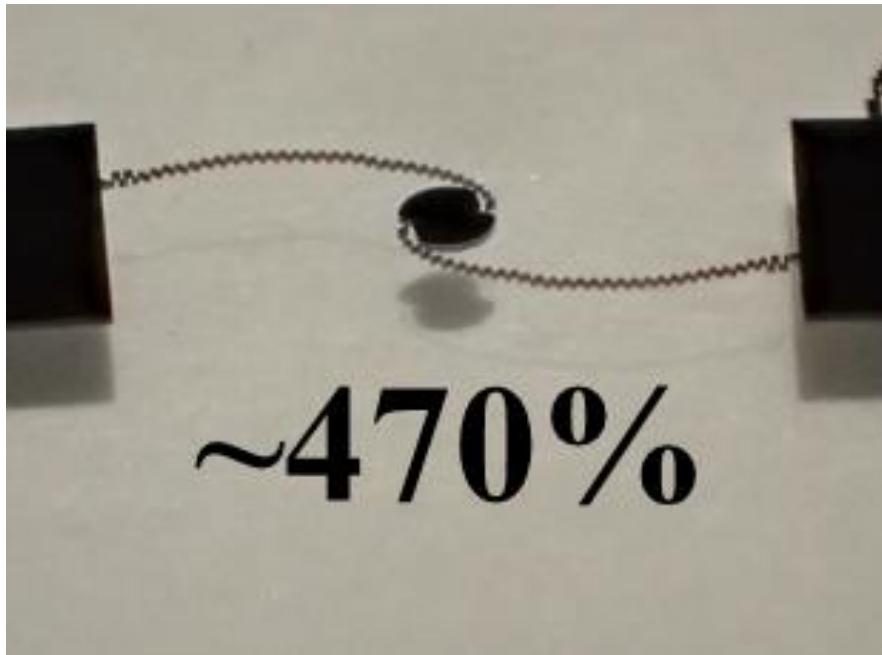


Figure 45 Stretched spiral between two Square Islands.

## CHAPTER

# CONCLUSION AND FUTURE WORK

Flexible and stretchable electronics are the future of the biomedical electronic industry. Several challenges are still out there to compete with the dominant market of rigid and brittle silicon based electronics in the market. In this research work we studied several variants of spiral-serpentine structures and studied the mechanical response of each of the proposed structures. Moreover, the weak areas (with maximum stress localized) were identified and then efforts were made to minimize the stress through geometrical modifications. The process was systematic, where each previous structure provided a base for next modification. Through this approach, the design was improved in a gradual manner. At the end a very efficient spiral-serpentine-horseshoe compound structure was proposed and studied for its mechanical response. Simulation results showed an outstanding decrease of ~55% in the stress value as compared to the structure with straight spiral arms. Moreover, further improvements can be made by adding horseshoe structures at the arms' starting and ending points, at the cost of more area. These results showed the remarkable potential of combining structures to optimize their mechanical behavior, thus accomplishing more robust platforms that will leverage the development of stretchable electronics.

This research work also provided the fabrication flow for two kind of wafers SOI and Si <100>. The SEM images show the effectiveness of the process to fabricate the flexible devices. Moreover, one of the fabricated structure was analyzed for its mechanical performance where the effectiveness of the proposed design and fabrication process was validated by stretching the structure to almost 470%. In summary, smart design of optimized compound structures can lead to efficient

interconnection schemes for stretchable electronics with area efficiency and better mechanical robustness and reliability. Also, extra stretchable structures can be fabricated using the brittle and rigid silicon by optimizing the involved processes and decreasing the arms' thickness.

The proposed/ fabricated structures can be used with actual electronic applications as stretchable interconnects, where the islands will host electronic active devices. Thus, the spirals can be used as electrical interconnections by the deposition of a metallic film using electrochemical deposition of a conductive material. This can lead the way to future applications in the field of bioelectronics, robotics and cybernetics.

Future work includes the mechanical characterization of the fabricated structures. It includes studying the effect of stress location in the actual fabricated structure and to evaluate the mechanical performance at different stretch ratios. Moreover, the final objective is to use these structures with actual electronic devices, where islands will host electronic devices and the spirals will act as conductive interconnects between islands.

## REFERENCES

- [1] S. Choi, H. Lee, R. Ghaffari, T. Hyeon, and D. H. Kim, “Recent Advances in Flexible and Stretchable Bio-Electronic Devices Integrated with Nanomaterials,” *Adv. Mater.*, vol. 28, no. 22, pp. 4203–4218, 2016.
- [2] D. Rus and M. T. Tolley, “Design, fabrication and control of soft robots,” *Nature*, vol. 521, no. 7553, pp. 467–475, 2015.
- [3] A. M. Hussain and M. M. Hussain, “CMOS-Technology-Enabled Flexible and Stretchable Electronics for Internet of Everything Applications,” *Adv. Mater.*, vol. 28, no. 22, pp. 4219–4249, 2016.
- [4] Y. Khan, A. E. Ostfeld, C. M. Lochner, A. Pierre, and A. C. Arias, “Monitoring of Vital Signs with Flexible and Wearable Medical Devices,” *Adv. Mater.*, vol. 28, no. 22, pp. 4373–4395, 2016.
- [5] M. Y. Cheng, C. M. Tsao, Y. Z. Lai, and Y. J. Yang, “The development of a highly twistable tactile sensing array with stretchable helical electrodes,” *Sensors Actuators, A Phys.*, vol. 166, no. 2, pp. 226–233, 2011.
- [6] E. S. Hwang, J. H. Seo, and Y. J. Kim, “A polymer-based flexible tactile sensor for both normal and shear load detections and its application for robotics,” *J. Microelectromechanical Syst.*, vol. 16, no. 3, pp. 556–563, 2007.
- [7] C. Wang *et al.*, “User-interactive electronic skin for instantaneous pressure visualization,” *Nat Mater*, vol. 12, no. 10, pp. 899–904, 2013.
- [8] A. E. Ostfeld, A. M. Gaikwad, Y. Khan, and A. C. Arias, “High-performance flexible energy storage and harvesting system for wearable electronics,” *Sci. Rep.*, vol. 6, no. April, p. 26122, 2016.
- [9] D.-H. Kim, N. Lu, Y. Huang, and J. a. Rogers, “Materials for stretchable electronics in bioinspired and biointegrated devices,” *MRS Bull.*, vol. 37, no. 3, pp. 226–235, 2012.
- [10] J. A. Rogers, T. Someya, and Y. Huang, “Materials and Mechanics for Stretchable Electronics,” *Science (80- )*, vol. 327, no. 5973, pp. 1603–1607, 2010.
- [11] M. A. Escabi *et al.*, “A high-density, high-channel count, multiplexed ECoG array for auditory-cortex recordings,” *J. Neurophysiol.*, vol. 112, no. 6, pp. 1566–1583, 2014.
- [12] N. Lu and D.-H. Kim, “Flexible and Stretchable Electronics Paving the Way for Soft Robotics,” *Soft Robot.*, vol. 1, no. 1, pp. 53–62, 2014.

- [13] K. D. Harris, A. L. Elias, and H. J. Chung, “Flexible electronics under strain: a review of mechanical characterization and durability enhancement strategies,” *J. Mater. Sci.*, vol. 51, no. 6, pp. 2771–2805, 2016.
- [14] Y. Sun and J. A. Rogers, “Inorganic semiconductors for flexible electronics,” *Adv. Mater.*, vol. 19, no. 15, pp. 1897–1916, 2007.
- [15] D. H. Kim, J. L. Xiao, J. Z. Song, Y. G. Huang, and J. A. Rogers, “Stretchable, curvilinear electronics based on inorganic materials,” *Adv. Mater.*, vol. 22, 2010.
- [16] D. Roylance, “Stress-Strain Curves,” *Department of Materials Science and Engineering Massachusetts Institute of Technology*, no. August. p. 2001, 2001.
- [17] W. Callister and D. Rethwisch, *Materials science and engineering: an introduction*, vol. 94. 2007.
- [18] Y. Leterrier *et al.*, “Mechanical integrity of transparent conductive oxide films for flexible polymer-based displays,” *Thin Solid Films*, vol. 460, no. 1–2, pp. 156–166, 2004.
- [19] Y. Leterrier *et al.*, “Mechanical integrity of thin inorganic coatings on polymer substrates under quasi-static, thermal and fatigue loadings,” *Thin Solid Films*, vol. 519, no. 5, pp. 1729–1737, 2010.
- [20] Z. Jia, M. B. Tucker, and T. Li, “Failure mechanics of organic-inorganic multilayer permeation barriers in flexible electronics,” *Compos. Sci. Technol.*, vol. 71, no. 3, pp. 365–372, 2011.
- [21] H. Chen, B. W. Lu, Y. Lin, and X. Feng, “Interfacial failure in flexible electronic devices,” *IEEE Electron Device Lett.*, vol. 35, no. 1, pp. 132–134, 2014.
- [22] V. Brand, C. Bruner, and R. H. Dauskardt, “Cohesion and device reliability in organic bulk heterojunction photovoltaic cells,” *Sol. Energy Mater. Sol. Cells*, vol. 99, pp. 182–189, 2012.
- [23] T. Someya *et al.*, “Conformable, flexible, large-area networks of pressure and thermal sensors with organic transistor active matrixes,” *Proc. Natl. Acad. Sci. U. S. A.*, vol. 102, no. 35, pp. 12321–12325, 2005.
- [24] S. J. Benight, C. Wang, J. B. H. Tok, and Z. Bao, “Stretchable and self-healing polymers and devices for electronic skin,” *Prog. Polym. Sci.*, vol. 38, no. 12, pp. 1961–1977, 2013.
- [25] T. Someya, T. Sekitani, S. Iba, Y. Kato, H. Kawaguchi, and T. Sakurai, “A large-area, flexible pressure sensor matrix with organic field-effect transistors for artificial skin applications,” *Proc. Natl. Acad. Sci. U. S. A.*, vol. 101, no. 27, pp. 9966–9970, 2004.

- [26] S. R. Forrest, “The path to ubiquitous and low-cost organic electronic appliances on plastic Stephen,” pp. 911–918.
- [27] N. T. Kalyani and S. J. Dhoble, “Organic light emitting diodes: Energy saving lighting technology — A review,” *Renew. Sustain. Energy Rev.*, vol. 16, no. 5, pp. 2696–2723, 2012.
- [28] J. P. Rojas, A. Arevalo, I. G. Foulds, and M. M. Hussain, “Design and characterization of ultra-stretchable monolithic silicon fabric,” *Appl. Phys. Lett.*, vol. 105, no. 15, 2014.
- [29] J. M. Nassar, J. P. Rojas, A. M. Hussain, and M. M. Hussain, “From stretchable to reconfigurable inorganic electronics,” *Extrem. Mech. Lett.*, vol. 9, pp. 245–268, 2016.
- [30] a. Nathan *et al.*, “Flexible Electronics: The Next Ubiquitous Platform,” *Proc. IEEE*, vol. 100, no. Special Centennial Issue, pp. 1486–1517, 2012.
- [31] Y. Yuan *et al.*, “Ultra-high mobility transparent organic thin film transistors grown by an off-centre spin-coating method,” *Nat. Commun.*, vol. 5, pp. 1–9, 2014.
- [32] S. Yao and Y. Zhu, “Nanomaterial-enabled stretchable conductors: Strategies, materials and devices,” *Adv. Mater.*, vol. 27, no. 9, pp. 1480–1511, 2015.
- [33] S. Park, M. Vosguerichian, and Z. Bao, “A review of fabrication and applications of carbon nanotube film-based flexible electronics,” *Nanoscale*, vol. 5, no. 5, pp. 1727–1752, 2013.
- [34] S. Araby, Q. Meng, L. Zhang, I. Zaman, P. Majewski, and J. Ma, “Elastomeric composites based on carbon nanomaterials.,” *Nanotechnology*, vol. 26, no. 11, p. 112001, 2015.
- [35] T. Sekitani *et al.*, “Stretchable active-matrix organic light-emitting diode display using printable elastic conductors,” *Nat. Mater.*, vol. 8, no. 6, pp. 494–499, 2009.
- [36] T. Sekitani, Y. Noguchi, K. Hata, T. Fukushima, T. Aida, and T. Someya, “A Rubberlike Stretchable Active Matrix Using Elastic ConductorsA Rubberlike Stretchable Active Matrix Using Elastic Conductors,” vol. 321, no. September, pp. 1468–1472, 2008.
- [37] S. J. Kang *et al.*, “High-performance electronics using dense, perfectly aligned arrays of single-walled carbon nanotubes.,” *Nat. Nanotechnol.*, vol. 2, no. 4, pp. 230–236, 2007.
- [38] Q. Cao and J. a. Rogers, “Random networks and aligned arrays of single-walled carbon nanotubes for electronic device applications,” *Nano Res.*, vol. 1, no. 4, pp. 259–272, 2008.
- [39] N. O. Weiss *et al.*, “Graphene: An emerging electronic material,” *Advanced Materials*, vol. 24, no. 43. pp. 5782–5825, 2012.
- [40] C. F. Guo and Z. Ren, “Flexible transparent conductors based on metal nanowire networks,” *Mater. Today*, vol. 18, no. 3, pp. 143–154, 2015.

- [41] C. Wang *et al.*, “Extremely Bendable, High Performance Integrated Circuits Using Semiconducting Carbon Nanotube Networks for Digital, Analog, and Radio-Frequency Applications,” *Nano Lett.*, vol. 12, pp. 1527–1533, 2012.
- [42] S. Zhu *et al.*, “Ultrastretchable fibers with metallic conductivity using a liquid metal alloy core,” *Adv. Funct. Mater.*, vol. 23, no. 18, pp. 2308–2314, 2013.
- [43] S. Il Park, J. H. Ahn, X. Feng, S. Wang, Y. Huang, and J. A. Rogers, “Theoretical and experimental studies of bending of inorganic electronic materials on plastic substrates,” *Adv. Funct. Mater.*, vol. 18, no. 18, pp. 2673–2684, 2008.
- [44] W. M. Choi, J. Song, D. Y. Khang, H. Jiang, Y. Y. Huang, and J. A. Rogers, “Biaxially stretchable ‘wavy’ silicon nanomembranes,” *Nano Lett.*, vol. 7, no. 6, pp. 1655–1663, 2007.
- [45] Y. Y. Huang and J. A. Rogers, “Biaxially Stretchable ‘Wavy’ Silicon Nanomembranes on Elastomeric Supports Fabricated,” *Mrs Bull.*, vol. 32, 2007.
- [46] J. A. Rogers, “Materials for semiconductor devices that can bend, fold, twist, and stretch,” *Mrs Bull.*, vol. 39, no. 6, pp. 549–556, 2014.
- [47] D. H. Kim, J. Xiao, J. Song, Y. Huang, and J. A. Rogers, “Stretchable, curvilinear electronics based on inorganic materials,” *Adv. Mater.*, vol. 22, no. 19, pp. 2108–2124, 2010.
- [48] Y. Sun, V. Kumar, I. Adesida, and J. A. Rogers, “Buckled and wavy ribbons of GaAs for high-performance electronics on elastomeric substrates,” *Adv. Mater.*, vol. 18, no. 21, pp. 2857–2862, 2006.
- [49] J. Jones, S. P. Lacour, S. Wagner, and Z. Suo, “Stretchable wavy metal interconnects,” *J. Vac. Sci. Technol. A Vacuum, Surfaces, Film.*, vol. 22, no. 2004, p. 1723, 2004.
- [50] T. Li, Z. Huang, Z. Suo, S. P. Lacour, and S. Wagner, “Stretchability of thin metal films on elastomer substrates,” *Appl. Phys. Lett.*, vol. 85, no. 16, pp. 3435–3437, 2004.
- [51] P. Mandlik, S. P. Lacour, J. W. Li, S. Y. Chou, and S. Wagner, “Fully elastic interconnects on nanopatterned elastomeric substrates,” *IEEE Electron Device Lett.*, vol. 27, no. 8, pp. 650–652, 2006.
- [52] S. P. Lacour, C. Tsay, and S. Wagner, “An elastically stretchable TFT Circuit,” *IEEE Electron Device Lett.*, vol. 25, no. 12, pp. 792–794, 2004.
- [53] D. S. Gray, J. Tien, and C. S. Chen, “High-Conductivity Elastomeric Electronics (Adv. Mater. 2004, 16, 393.),” *Adv. Mater.*, vol. 16, no. 6, pp. 477–477, 2004.
- [54] H. Fu *et al.*, “Lateral buckling and mechanical stretchability of fractal interconnects partially bonded onto an elastomeric substrate,” *Appl. Phys. Lett.*, vol. 106, no. 9, 2015.

- [55] Y. Su, Z. Liu, S. Kim, J. Wu, Y. Huang, and J. A. Rogers, “Mechanics of stretchable electronics with high fill factors,” *Int. J. Solids Struct.*, vol. 49, no. 23–24, pp. 3416–3421, 2012.
- [56] D. H. Kim *et al.*, “Optimized structural designs for stretchable silicon integrated circuits,” *Small*, vol. 5, no. 24, pp. 2841–2847, 2009.
- [57] D.-H. Kim *et al.*, “Materials and noncoplanar mesh designs for integrated circuits with linear elastic responses to extreme mechanical deformations,” *Proc. Natl. Acad. Sci. U. S. A.*, vol. 105, no. 48, pp. 18675–18680, 2008.
- [58] J. a Fan *et al.*, “Fractal design concepts for stretchable electronics,” *Nat. Commun.*, vol. 5, p. 3266, 2014.
- [59] Z. Yan *et al.*, “Mechanical assembly of complex, 3D mesostructures from releasable multilayers of advanced materials,” *Sci. Adv.*, vol. 2, no. 9, p. e1601014, 2016.
- [60] S. Xu *et al.*, “Assembly of micro/nanomaterials into complex, three-dimensional architectures by compressive buckling,” *Science (80-.)*, vol. 347, no. 6218, pp. 154–159, 2015.
- [61] C. Lv, H. Yu, and H. Jiang, “Archimedean spiral design for extremely stretchable interconnects,” *Extrem. Mech. Lett.*, vol. 1, pp. 29–34, 2014.
- [62] K. Huang *et al.*, “An approach to cost-effective, robust, large-area electronics using monolithic silicon,” *Tech. Dig. - Int. Electron Devices Meet. IEDM*, pp. 217–220, 2007.
- [63] A. Mamidanna, Z. Song, C. Lv, C. S. Lefky, H. Jiang, and O. J. Hildreth, “Printing Stretchable Spiral Interconnects Using Reactive Ink Chemistries,” *ACS Appl. Mater. Interfaces*, vol. 8, no. 20, pp. 12594–12598, 2016.
- [64] J. P. Rojas, D. Singh, D. Conchouso, A. Arevalo, I. G. Foulds, and M. M. Hussain, “Stretchable Helical Architecture Inorganic-Organic Hetero Thermoelectric Generator,” *Nano Energy*, vol. 30, no. October, p. DOI: 10.1016/j.nanoen.2016.10.054, 2016.
- [65] K.-I. Jang *et al.*, “Rugged and breathable forms of stretchable electronics with adherent composite substrates for transcutaneous monitoring,” *Nat. Commun.*, vol. 5, p. 4779, 2014.
- [66] P. J. Hung, K. Jeong, G. L. Liu, and L. P. Lee, “Microfabricated suspensions for electrical connections on the tunable elastomer membrane,” *Appl. Phys. Lett.*, vol. 85, no. 24, pp. 6051–6053, 2004.
- [67] W. S. Wong and A. Salleo, *Flexible Electronics: Materials and Applications*, vol. 1. Springer US, 2009.
- [68] H. C. Ko, A. J. Baca, and J. A. Rogers, “Bulk Quantities of Single-Crystal Silicon Micro-



- / Nanoribbons Generated from Bulk Wafers,” 2006.
- [69] J. Yoon *et al.*, “Ultrathin silicon solar microcells for semitransparent, mechanically flexible and microconcentrator module designs,” *Nat. Mater.*, vol. 7, no. 11, pp. 907–915, 2008.
- [70] J. H. Ahn *et al.*, “High-speed mechanically flexible single-crystal silicon thin-film transistors on plastic substrates,” *IEEE Electron Device Lett.*, vol. 27, no. 6, pp. 460–462, 2006.
- [71] L. Sun, G. Qin, J. H. Seo, G. K. Celler, W. Zhou, and Z. Ma, “12-GHz thin-film transistors on transferrable silicon nanomembranes for high-performance flexible electronics,” *Small*, vol. 6, no. 22, pp. 2553–2557, 2010.
- [72] J. H. Ahn *et al.*, “Bendable integrated circuits on plastic substrates by use of printed ribbons of single-crystalline silicon,” *Appl. Phys. Lett.*, vol. 90, no. 21, pp. 88–91, 2007.
- [73] J. P. Rojas *et al.*, “Transformational silicon electronics,” *ACS Nano*, vol. 8, no. 2, pp. 1468–1474, 2014.
- [74] D. Shahrjerdi and S. W. Bedell, “Extremely flexible nanoscale ultrathin body silicon integrated circuits on plastic,” *Nano Lett.*, vol. 13, no. 1, pp. 315–320, 2013.
- [75] J. P. Rojas, A. Syed, and M. M. Hussain, “Mechanically Flexible Optically Transparent Porous Mono-Crystalline Silicon Substrate,” in *Micro Electro Mechanical Systems (MEMS)*, 2012, no. February, pp. 281–284.
- [76] J. P. Rojas and M. M. Hussain, “Flexible semi-transparent silicon (100) fabric with high-k/metal gate devices,” *Phys. Status Solidi - Rapid Res. Lett.*, vol. 7, no. 3, pp. 187–191, 2013.
- [77] J. P. Rojas, G. Torres Sevilla, and M. M. Hussain, “Structural and electrical characteristics of high-k/metal gate metal oxide semiconductor capacitors fabricated on flexible, semi-transparent silicon (100) fabric,” *Appl. Phys. Lett.*, vol. 102, no. 6, 2013.
- [78] T. Widlund, S. Yang, Y. Y. Hsu, and N. Lu, “Stretchability and compliance of freestanding serpentine-shaped ribbons,” *Int. J. Solids Struct.*, vol. 51, no. 23–24, pp. 4026–4037, 2014.
- [79] Z. Fan *et al.*, “A finite deformation model of planar serpentine interconnects for stretchable electronics,” *Int. J. Solids Struct.*, vol. 91, pp. 46–54, 2016.
- [80] Q. Ma *et al.*, “A nonlinear mechanics model of bio-inspired hierarchical lattice materials consisting of horseshoe microstructures,” *J. Mech. Phys. Solids*, vol. 90, pp. 179–202, 2016.
- [81] Q. Ma *et al.*, “Mechanics of Fractal-Inspired Horseshoe Microstructures for Applications

in Stretchable Electronics,” *J. Appl. Mech.* 83 (2017) 111008-111027.  
doi:10.1115/1.4034458.

- [82] M. A. Hopcroft *et al.*, “What is the Young's Modulus of Silicon?,” *J. Microelectromech. Syst.*, 19 (2010) 229-238. doi: 10.1109/JMEMS.2009.2039697

# Vitae

**Name:** Mutee Ur Rehman

**Nationality:** Pakistani

**Date of Birth:** 04/27/1989

**Email:** muteeurehman@gmail.com

**Address:** Village and Post office Mirpur District & Tehsil Haripur

## Academic Background:

**King Fahd University of Petroleum and Minerals, Dhahran, Saudi Arabia (2015-2017)**

*M.Sc. Electrical Engineering- (Electronics)*

Thesis Title: Optimization of Spiral-based Structures for Stretchable Electronics

**Mohammad Ali Jinnah University, Islamabad, Pakistan (2007 – 2011)**

*B.Sc. Electronics Engineering*

Thesis Title: Deployment of IEEE 802.11n and Its Use in Controlling Security Camera.

## Publications:

- [1] M.U. Rehman, J.P. Rojas, "Folding and Stretching a Thermoelectric Generator ", In SPIE Defense+ Security, pp. International Society for Optics and Photonics, 2018
- [2] M.U. Rehman, Galo A. Torres Sevilla, M. M. Hussain, J.P. Rojas, "Development of Highly Stretchable Fractal Inspired Silicon-Based Compound Structures", Materials Research Society(MRS), 2017. (Poster Presentation)
- [3] N. Qaiser, S. Khan, M. Nour, M. U. Rehman, J. P. Rojas, M. M. Hussain," Mechanical Response of Spiral Interconnect Arrays for Highly Stretchable Electronics" Appl. Phys. Lett. 111, 214102 (2017).
- [4] M.U. Rehman, J.P. Rojas, "Optimization of Compound Serpentine-Spiral Structure for Ultra-Stretchable Electronics", Extrem. Mech. Lett. 2017.
- [5] M.Rehman, M.Drieberg, N.Badruddin, "Probabilistic Polling MAC Protocol with Unslotted CSMA for Wireless Sensor Networks (WSNs) ", in 5th Int. Conf. Intell. Adv. Syst. (ICIAS), June 2014.